Acceptance times Efficiency corrections for Upsilon(1S) production in proton-proton collisions at 5.02 TeV

T H E S I S

Submitted in partial fulfillment of the requirements for the degree of

BACHELOR'S DEGREE IN PHYSICS

in the

DEPARTMENT OF PHYSICS

of the

UNIVERSITY OF SONORA

by

JOSÉ DANIEL GAYTÁN VILLARREAL

THESIS ADVISOR
PhD Lizardo Valencia Palomo

May 2022

Correcciones de Aceptancia por Eficiencia para la producción de Upsilon(1S) en colisiones protón-protón a 5.02 TeV

T E S I S

Presentada como satisfacción parcial de los requerimientos para el título de

LICENCIADO EN FÍSICA

del

DEPARTAMENTO DE FÍSICA

de la

UNIVERSIDAD DE SONORA

por

JOSÉ DANIEL GAYTÁN VILLARREAL

DIRECTOR DE TESIS
Dr. Lizardo Valencia Palomo

Mayo 2022

”*La science, mon garçon, est faite d’erreurs, mais d’erreurs qu’il est bon de commettre, car elles mènent peu à peu à la vérité* ”,
Jules Verne, *Voyage au centre de la terre*.

”*Truth emerges more readily from error than from confusion*”,
Thomas Kuhn, *The Structure of Scientific Revolutions*.

Agradecimientos
Acknowledgments

Esta página es lo último que escribo de esta tesis, pues es para mí la parte más difícil; esto se debe a que tengo la buena (mala) suerte de tener más personas a las que agradecer en mi vida de las que puedo plasmar en una página. Espero poder hacer justicia a todas esas personas que con su ayuda, guía, tutela, o su mera compañía, hicieron posible la realización de este trabajo, y de antemano pido disculpas si alguien se siente omitido. Les aseguro que no es así. Procedo, pues, a agradecer.

A mis padres, quienes si bien no siempre me han entendido ni a mí ni a las decisiones que he tomado, han estado allí para apoyarme y ayudarme a seguir mi camino.

Al Dr. Lizardo Valencia, cuya valiosa tutela estos últimos ocho meses hizo posible todo este proyecto y me permitió aprender un sin fin de cosas sobre esta interesante rama de la física.

A mi hermana y hermano, a mis tíos, tías, primos, primas, mi abue y a toda mi familia, pues es gracias a su cariño y apoyo que siempre he podido salir adelante.

A todos mis amigos y amigas, quienes siempre están allí para darme ánimos y risas y hacer que todo este trabajo valga la pena.

A la comunidad de física, a mis profesoras y profesores, a mis amigos y amigas, compañeros y compañeras, por hacer de esta carrera un segundo hogar.

Por último, a mi tata y a mi nana, quienes me formaron para ser el hombre que soy ahora al enseñarme el verdadero valor del conocimiento. Donde sea que estén, los quiero.

Contents

List of Figures

List of Tables

Abstract

At high energy and temperature densities ordinary nuclear matter undergoes a phase transition, where quarks and gluons, originally confined inside hadrons, are now free. This new state of matter, believed to have existed in the first instants after the Big Bang, is known as Quark Gluon Plasma. This plasma is recreated in the lab using high energy heavy ion collisions and is studied using indirect measurements techniques, such as quarkonium (heavy quark-antiquark bound states) suppresion.

Before doing the study in nuclear collisions, it is necessary to quantify the production of particles in proton-proton collisions. One of the principal components of this study is the Acceptance and Efficiency corrections, since these take into account the geometrical and functional limitations of the detector.

In this work the results of Acceptance and Efficiency in the production of Upsilon(1S) in proton-proton collisions at 5.02 from the CMS experiment at LHC are presented.

Resumen

A altas densidades de energía y temperatura la materia nuclear ordinaria sufre una transformación de fase, donde los quarks y gluones originalmente confinados en los hadrones se encuentran libres. A este nuevo estado de la materia, que se cree existió en los primeros instantes después del Big Bang, se le conoce como Plasma de Quarks y Gluones. En el laboratorio se recrea este plasma usando colisiones de iones pesados y se estudia por medio de mediciones indirectas. Una de éstas es la supresión de quarkonium (estados ligados de quark-antiquark pesados) debido al desconfinamiento de quarks y gluones.

Antes de realizar el estudio en colisiones nucleares, es necesario cuantificar la producción de partículas en colisiones protón-protón. Uno de los componentes de estos estudios es la corrección de aceptancia y eficiencia, que toma en cuenta las limitaciones geométricas y de funcionamiento del detector.

En este trabajo se presentan los resultados de aceptancia y eficiencia en la producción de Upsilon (1S) en colisiones protón-protón a 5.02 TeV en el experimento CMS del LHC.

Introduction

The present thesis is the fruit of my work under PhD Lizardo Valencia mentorship for the span of approximately eight months. This is but an undergraduate understanding of particle physics: to those more familiar with the field, I beg you forgive my shortcomings; to those who are not but, like myself, are eager to learn, I hope this work serves as a small guide as to where to start looking.

The present work focuses on the calculations of the Acceptance and Efficiency of a GEANT4 simulation from the CMS detector; this is part of a broader, more complete analysis being done by a group of physicists at the CMS experiment.

Chapter 1 provides a concise explanation of the Standard Model, the most complete model to date used by particle physicists to explain the composition of the universe, followed by a small explanation of the creation of new particles in proton-proton collisions. Finally, the concept of bound states is introduced, as a foreword to the main body of this work: quarkonium, more specifically a bottomonium state known as the Upsilon Υ (1S) particle.

Chapter 2 briefly describes the experimental aparatus used by particle physicists to measure particles, the CERN's accelerator complex; it then goes into a deeper explanation of the detector used in this work, the CMS CERN experiment, describing its components and functions in a detailed manner.

Chapter 3 explains the methodology used during the elaboration of this thesis, describing how the Acceptance and Efficiency were calculated, as well as the statistical procedures applied to these results.

Chapter 4 shows the results obtained for each of the methods applied, as well as giving an small statistical interpretation.

Chapter 5 puts an end to the work by giving the corresponding conclusions obtained, and also exposing the further work that is yet to be done to improve on the work done.

As final words to this introduction, I hope that this thesis serves as a small beacon of knowledge for anyone who wishes to dive further in this interesting area of physics, and thank whoever takes the time to go through my work.

Introducción

La presente tesis es el fruto de mi trabajo bajo la tutela del Dr. Lizardo Valencia durante el transcurso de aproximadamente ocho meses. Decidí escribirla en inglés debido a que, nos guste o no, el inglés es el idioma de las ciencias. Este trabajo no es más que el entendimiento de un estudiante de licenciatura en física de la física de partículas: para aquellos más familiarizados con el área, les pido perdonen mi falta de conocimiento; para aquellos que no lo son pero, como yo, están deseosos de aprender, espero que este trabajo les sirva como una pequeña guía de dónde empezar a buscar.

El presente trabajo se enfoca en los cálculos de Aceptancia y Eficiencia de una simulación de GEANT4 del detector CMS; esto es parte de un análisis más amplio y completo realizado al mismo tiempo por un grupo de físicos en el experimento CMS.

El capítulo 1 da una concisa descripción del Modelo Estándar, el modelo más completo a la fecha usado por los físicos de partículas para explicar la composición del universo, seguido por una explicación de la creación de nuevas partículas en colisiones protón-protón. Finalmente, se introduce el concepto de estados ligados mediante un estado de quarkonium, el bottomonium, conocido como la partícula Upsilon Υ (1S).

El capítulo 2 describe brevemente el aparato experimental utilizado por los físicos de partículas, el complejo de aceleradores del CERN; le sigue una explicación más profunda del detector cuya respuesta fue simulada en este trabajo, el experimento CMS del CERN, describiendo sus componentes y funciones de manera detallada.

El capítulo 3 explica la metodología utilizada para la realización del estudio presentado a través de la presente tesis, describiendo como es que fueron calculadas la Aceptancia y Eficiencia, así como los procesos estadísticos que se aplicaron a estos resultados.

El capítulo 4 muestra los resultados obtenidos para cada método aplicado, así como breves interpretaciones estadísticas.

El capítulo 5 pone fin a este trabajo al dar las conclusiones correspondientes, además de exponer el trabajo a futuro por realizarse para mejorar el trabajo hecho.

Como últimas palabras a esta introducción, espero que esta tesis sirva como un pequeño faro de conocimiento para quien desee profundizar más en esta interesante área de la física, y agradezco a quien se haya tomado el tiempo de leer mi trabajo.

CHAPTER 1
Theoretical Background

Through history, humanity has yearned to answer the question: what is the universe made of? Multiple answers have been given, and progress has been made towards the truth: from the conception of the idea of the atom by Democritus [1], to Mendeleev's periodic table [2], it could be said that we understand the composition of matter, or at least of the currently observable matter. That would be the case, *if atoms were actually the fundamental constituents of matter*; in reality, they are composed of more fundamental pieces, called *elementary particles*. The area of physics that studies these particles is called Particle Physics, and the theory that physicists use to study and classify these particles is known as The Standard Model.

1.1 The Standard Model

The Standard Model (SM) is the most complete theory to date that explains the particles that compose our universe and the physical interactions that reign over them. It has been proved experimentally in many occasions, and it has even predicted experimental results that weren't possible to prove due to technological constraints at the time [3]. It has, however, several limitations, which are currently being explored in research known as Beyond the Standard Model Physics [4], but these will not be discussed in this work.

According to the SM, all matter is made out of two types of elementary particles: fermions, divided into quarks and leptons, and bosons, which mediate the forces between the fermions. This totals to three kinds of particles, which interact through four fundamental forces: strong, weak, electromagnetic, and gravitational [5]; the latter is yet to be incorporated into the SM, since it has no measurable effects on a subatomic scale and as such the related boson has not been observed [6].

1.1.1 The fundamental particles

1.1.1.1 Fermions

As it was said before, fermions can be subdivided into two categories of particles: quarks and leptons. They do, however, share a set of common properties [7]:

- Semi-integer spin values $\left(\frac{1}{2}\hbar, \frac{3}{2}\hbar, \frac{5}{2}\hbar ... \frac{(2n+1)}{2}\hbar \forall n \in Z\right)$.
- Antisymmetric wave function.
- Organized in three families of particles, containing two ”flavors” of particles each, from least to most massive.
- Follows Fermi-Dirac statistics, thus obeys Dirac´s exclusion principle.

From the last property, it is derived that for every fermion, there exists an ”anti-fermion”, which shares the same properties of a fermion but has oposite electrical charge. It must also be noted that fermions, as all elementary particles, are point-like, for no internal structure has ever been observed [8].

The first type of fermions are called **quarks**. These type of fermions have two unique properties that differentiates them from leptons [7]:

- ”Color” charge.
- Semi-integer electrical charge value of the electron charge.

The first property, the ”color” charge, is the charge mediated by the strong force, and is analogous to the electric charge in electrodynamics, having three possible values, which are red, blue and green; as a consequence of this force, quarks are never seen as free particles in nature, being confined in bound states of quarks known as hadrons [4].

Quarks			
Family	Quark	Charge (e)	Mass (GeV)
1st Family	Up (u)	$+\frac{2}{3}$	0.005
	Down (d)	$-\frac{1}{3}$	0.003
2nd Family	Charm (s)	$+\frac{2}{3}$	1.3
	Strange (s)	$-\frac{1}{3}$	0.1
3rd Family	Top (t)	$+\frac{2}{3}$	174
	Bottom (b)	$-\frac{1}{3}$	4.5

Table 1.1: Properties of quarks [4]

Each one of the quarks shown in Table 1.1 have their respective antiquark (called antiup, antidown, etc.), which, as it has been said before, have the exact same properties but opposite sign charge, forming a total of 12 quarks [5].

The second type of fermions are called **leptons**. These type of fermions have two unique properties that differentiates them from quarks [7]:

- Particles can be charge-neutral.
- Integer electrical charge value of the electron charge.

The first property refers to the existence of neutrinos, a type of leptons that are (almost) massless particles with no electrical charge that only interact through the weak force so they rarely interact with matter, and as such are really hard to detect [9].

Leptons			
Family	Lepton	Charge (e)	Mass (GeV)
1st Family	Electron (e)	-1	0.0005
	Electronic Neutrino (ν_e)	0	$< 10^{-9}$
2nd Family	Muon (μ)	-1	0.106
	Muonic Neutrino (ν_μ)	0	$< 10^{-9}$
3rd Family	Tau (τ)	-1	1.78
	Tau Neutrino (ν_τ)	0	$< 10^{-9}$

Table 1.2: Properties of leptons [4].

Similar to quarks, all leptons shown in Table 1.2 have their respective antilepton (called antielectron, anti-electron neutrino, etc.), which, as it has been said before, have the exact same properties but opposite sign charge, forming a total of 12 leptons [5].

1.1.1.2 Bosons

Bosons, also known as *gauge bosons*, or simply *mediator particles*, are the particles responsible for the fundamental interactions between fermions; essentially, they work as mediators, ”carrying” one type of force from a fermion to another, thus generating the interactions [4].

These particles share a common set of properties that identifies them as bosons [7]:

- Integer spin values $(0, \hbar, 2\hbar, ...)$
- Follows Bose-Einstein statistics.
- Symmetrical wave function.

Bosons			
Mediated force	Boson	Charge (e)	Mass (GeV)
Strong	Gluon (g)	0	0
Electromagnetic	Photon (γ)	0	0
Weak	$W^{\pm}$ Boson Z^0 Boson	± 1 0	80.40 91.18

Table 1.3: Properties of bosons [4].

1.1.2 The fundamental forces

The SM describes nature as having only four fundamental forces: strong, electromagnetic, weak, and gravitational [3] [9].

- **The Strong Force** is responsible for the binding of nuclei. Out of all the forces, it is the strongest (hence the name *strong* force), which explains how a proton is composed of three quarks bounded together. As seen in section 1.1.1.2, it's mediated by gluons, which can take up to three different color ”charges”, red, green, and blue, and only quarks are affected by it (see section 1.1.1.1).
- **The electromagnetic force**, a more commonly known force due to its macroscopic phenomena, is responsible for the electromagnetic interaction between all electrically charged particles. The boson responsible for mediating this force is the photon, as seen in section 1.1.1.2.

- **The weak force** is the one responsible for nuclear beta decay and similar decay processes of fundamental particles. This force is mediated through the W and Z bosons, as seen in section 1.1.1.2.

- **The gravitational force** is, evidently, the one responsible for gravitational interaction between two objects. At subatomic level, its effects are negligible, and, as mentioned in section 1.1.1.2, no related boson has been measured.

The reason that the strong and weak force are not observed at macroscopic level is due to its range, which, unlike electromagnetic and gravitational forces, ts not infinite, but rather minuscule [6].

Fundamental Forces				
Force	Range	Relative strength	Theory	Mediator
Strong	1fm	1	Chromodynamics	Gluon
Electromagnetic	∞	10^{-2}	Electrodynamics	Photon
Weak	10^{-3} fm	10^{-7}	Flavordynamics	W and Z
Gravitational	∞	10^{-38}	Geometrodynamics	Unknown

Table 1.4: The fundamental forces of nature [3] [5]

1.1.3 The fundamental interactions

There are three main theories that explain the interactions between the fundamental particles. Each of them can be described by their respective lagrangian, whose derivation will not be explained in this work.

1.1.3.1 Quantum Chromodynamics (QCD)

The complete Lagrangian for QCD is

$$\mathscr{L} = [i\hbar\overline{\psi}\gamma^{\mu}\partial_{\mu}\psi - mc^{2}\overline{\psi}\psi] - \frac{1}{16\pi}\mathbf{F}^{\mu\nu}\cdot\mathbf{F}_{\mu\nu} - (q\overline{\psi}\lambda\psi)\cdot\mathbf{A}_{\mu} \tag{1.1}$$

where γ^{μ} are the Dirac matrices, $\mathbf{F}_{\mu\nu}$ are the kinetic terms tensors, λ are the Gell-Mann matrices, and $\mathbf{A}_{\mu}$ are the gauge fields, one for each of the eight gluons.This equation is invariant under local SU(3) gauge transformations and describes three equal-mass Dirac fields, one for each color a gluon can take, that interact with eight massless vector fields, that is, the gluons [5] [10].

1.1.3.2 Quantum Electrodynamics (QED)

The complete Lagrangian for QED is

$$\mathscr{L} = \overline{\psi}(i\gamma^{\mu}\partial_{\mu} - m_e)\psi + e\overline{\psi}\gamma^{\mu}\psi\mathbf{A}_{\mu} - \frac{1}{4}\mathbf{F}_{\mu\nu}\cdot\mathbf{F}^{\mu\nu} \tag{1.2}$$

where γ^{μ} are the Dirac matrices, $\mathbf{A}_{\mu}$ is the covariant four-potential, and $\mathbf{F}_{\mu\nu}$ is the electromagnetic field tensor. This equation is invariant under U(1) local phase transformations [4]. As seen in section 1.1.1.2, the related bosons, photons, are massless [11] .

1.1.3.3 Electroweak Theory

Since, as seen in section 1.1.1.2, the bosons that mediate the weak force have mass, there was a need to incorporate the Higgs boson to fully explain the weak interactions. As such, instead of a standalone theory, it was needed to unify both electronic and weak interactions in what is known as Electroweak Theory (EWT).

The EWT Lagrangian is way too complicated and extensive for the scope of this work, so it will be omitted [12].

1.2 Proton-Proton Collisions

A diverse variety of experimental methods are used in particle physics to study these elementary particles [9]. One of the most common methods, and coincidentally one of the most intuitive, is particle-particle collisions, where two hadrons collide at relatively high energies in order to ”break” them into their elementary particles components, which in turn scatter into more elementary particles. In some cases, these types of collisions are known as *inelastic processes*, which means that the colliding hadrons lose a varying amount of their energies; in essence, this lost energy ”creates” new particles through a process known as **particle scattering** [13].

In this section, we will discuss an example of this method: the proton-proton (pp) collisions, which was the one used to gather the data for this work.

1.2.1 Properties of a proton

Discovered by Rutherford in 1917 by bombarding nitrogen molecules with helium-4 nucleus, protons were originally thought to be fundamental particles [14]; it is now known they are type of hadrons called baryons, composed of three-quark states qqq. The proton is then (ideally) a baryon whose valence quarks are two ups and one down, with a charge of +e, a semi-integer spin value, and an invariant mass of $m_p = 928MeV$ [7] [15].

Figure 1.1: Quark model of a proton [15].

It must be noted that while the aforementioned proton model serves for most calculations, for particle scatterings one may visualize the proton as a ”sea” of *partons*, which are a finite number of interacting groups of quarks and gluons inside the proton: when a proton collisions with another hadron, what is actually interacting are their partons. As such, when studying pp collisions, what we are actually studying are the partons-partons interactions of the protons [4] [14].

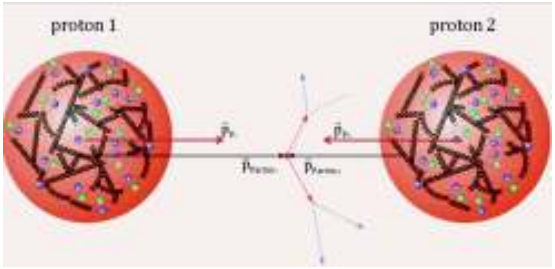

Figure 1.2: Partonic model of a pp collision [16].

1.2.2 Particle scattering: the creation of new particles

A particle scattering process can be described by three principal sub-processes [17]:

1. Two partons, i and j are extracted from each hadron with momentum fractions, according to the probabilities given by the *Parton Distribution Function* (PDF) $f_{i/j}(x_{i/j}, \mu_F^2)$, distribution functions that parametrize the transition of incident hadrons to incident partons based on the longitudinal momentum fraction x of partons with respect to the hadron taken at the factorization scale μ_F [10]. In probabilistic terms: $f_q(x)$ is the probability of finding a quark of flavor q that carries a momentum fraction x of the proton longitudinal momentum [16].

2. Heavy flavours, particles that contain at least one charm or bottom quark, are produced during hard scatterings, scatterings where the resulting particle has a transverse moment greater than 1 GeV, between the two extracted partons.

3. The formed heavy quark interacts with other partons and fragments into an open heavy flavour hadron.

These sub-processes will occur a varying number of times for each collision, depending on a variety of factors such as the energy at which each proton is accelerated, the angle of collision, or even completely random QCD-events; they will always, however, obey the conservation of energy [10]. These generated particles can then *decay* into other particles as they reach their lifespan, generating what are known as ”particle showers”; if these particles are generated through electromagnetic processes, they are known as electromagnetic showers; if they follow QCD processes, they are then known as hadronic showers [7]. There are a variety of methods through which these particles are measured; the ones used in this work will be discussed in chapter 2.

1.3 Bound States

It has been mentioned that particles are *bound states* of quarks. But what exactly are these ”bound states”? In quantum physics, a **bound state** is a quantum state of a particle subject to a potential, such that the particle has a tendency to remain in one or more regions of space [5]. In the following section, the mathematics behind this concept will be briefly explained, and a specific example will be given.

1.3.1 The Schrödinger equation

The Schrödinger equation is the basis for quantum theory. However, it is crucial to know if the system to be studied is relativistic or not, because the equation varies in each case. For reasons that will be explained in section 1.3.2, we are only interested in the three dimensional, time-independent, non-relativistic case, under the effects of an spherically symmetrical potential (as is the case in most quarks systems), and as such we define the non-relativistic time-independent radial Schrödinger equation as [18]

$$-\frac{\hbar^2}{2m}\frac{d^2\Psi}{dr^2}+\left[V(r)+\frac{\hbar^2}{2m}\frac{l(l+1)}{r^2}\right]\Psi=E\Psi \tag{1.3}$$

where l is known as the azimuthal quantum number. It describes the time evolution of the wave function $\Psi(r,t)$, describing a particle of mass m in the presence of an spherically symmetrical potential $V(r)$. This equation can be generalized to two-particle systems by simply using the reduced mass of two particles instead [5]. In these cases, the Schrödinger equation describes the time evolution of a *bound state* of two particles, which is the case concerning this work.

1.3.2 Quarkonia

The term *quarkonia*, plural for *quarkonium*, refers to mesons comprised of a heavy quark Q and its corresponding antiquark $\bar{Q}$; in other words, *bound states* mesons of a quark and its antiquark of quarks from the third family, bounded by the strong force. This term refers particularly to two ”families”: *charmonia* (bound states of a charm and an anticharm $c\bar{c}$), and ***bottomonia*** (bound states of a bottom and an antibottom $b\bar{b}$), as the top quark's mass is way too high for there to be a bound $t\bar{t}$ state [19].

There are a variety of production mechanisms for quarkonia. Since the simulated data for this work were taken from pp collisions as mentioned in section 1.2, only the case of hadron-hadron collisions will be acknowledged. At tree level in QCD, hadron-hadron interactions can produce quarkonia via two methods [20]:

- QCD-annihilation
- gluon fusion and splitting

From two production methods, quarkonia production can be segmented into two parts: first, an intermediate $Q\bar{Q}$ pair is produced at short distance, calculable within perturbative QCD; then, the hadronization occurs, which is just another term to call the formation of a QCD bound state [21]. It must be noted, though, that the second method listed is the dominant channel for quarkonia production, since inside the partons in each proton there is a large distribution of gluons [20].

Quarkonia systems can be treated as approximately non-relativistic, because the relative quark velocity in the bound states are relatively low in relation to the speed of light [21]. As such, equation 1.3 serves to calculate the energy levels of these bound states.

The quarkonia energy states can be obtained using equation 1.3. For this, we first calculate the reduced mass of the quarkonium system

$$\mu = \frac{m_q m_{\bar{q}}}{m_q + m_{\bar{q}}} = \frac{m_q}{2} \tag{1.4}$$

and we define the quarkonium potential as

$$V(r) = ar^2 + br - \frac{c}{r}, a > 0 \tag{1.5}$$

which is independent of quark flavor [14]. Note that it does not depends on time, as it was required when defining equation 1.3 [18].

From this point, there are a variety of methods to solve the Schrödinger equation for quarkonia, both numerical [22] and analytical [23] [24], but due to length constraints these will not be looked upon in this work.

1.3.2.1 Bottomonia

The quarkonium state of a bottom and an antibottom quark is known as *bottomonia* [21]. These bound states cover a relatively wide energy spectrum [25], and are actively looked for by particle physicists due to their probing qualities [19] [20] [21].

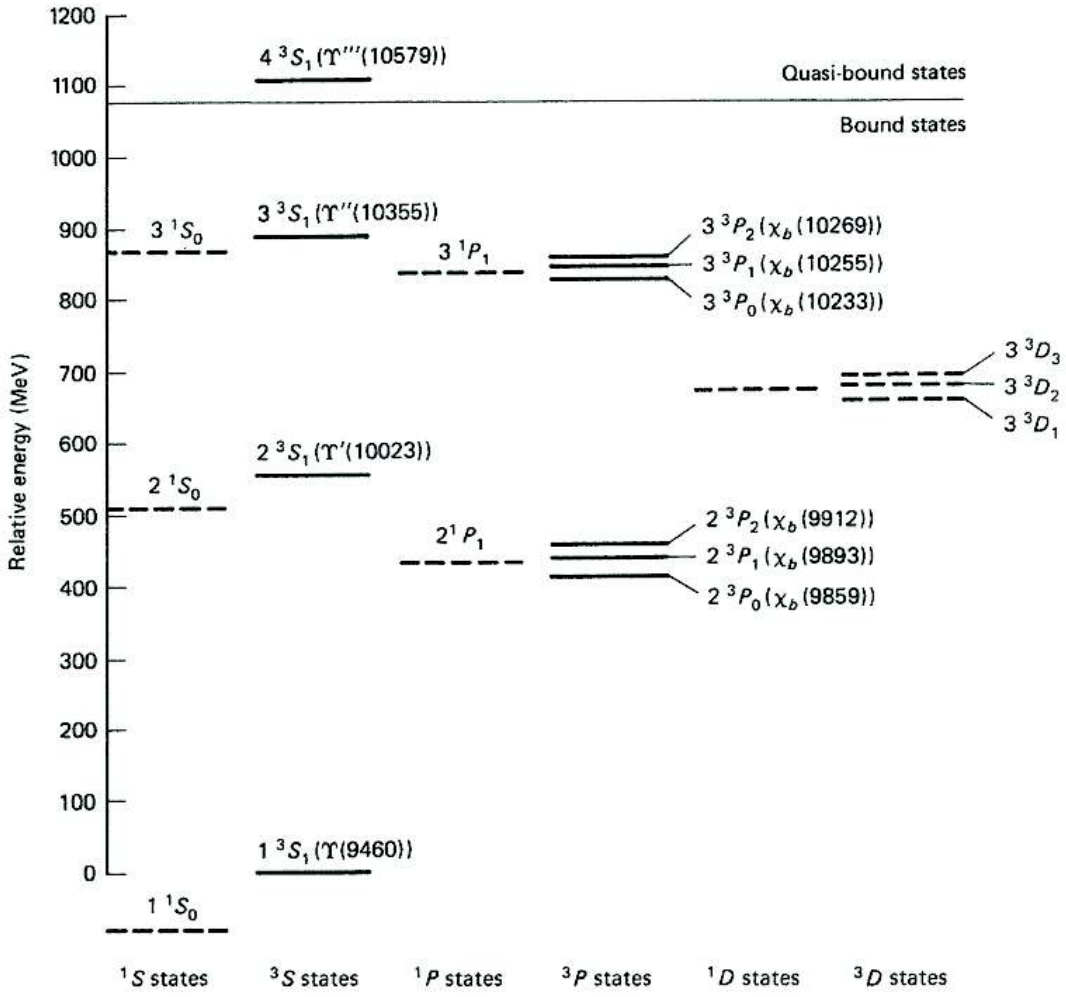

Figure 1.3: Bottomonium energy spectrum for all available bound states [5].

1.4 Upsilon Υ (1S)

The Upsilon Υ (1S) is the lowest energy state of the bottomonium mesons [9], and it is actively looked for by particle physicists due to its probing qualities [14]. In this section we will study this quarkonia state in more detail, focusing on its discovery, its physical properties and the detection methods and probing qualities it posses.

1.4.1 Discovery

The discovery of the charmonium meson J/Ψ in 1970 had sparked a search for heavier, non-relativistic states of heavier quarks: the chase for bottomonium had begun. It was not until 1977 that the first bottomonium mesons were discovered, detected as spin-triplet states (Υ (1S), Υ (2S) and Υ (3S)) by the E288 Collaboration at Fermilab in 1977, using proton scattering on *Cu* and *Pb* targets [25] [26] .

1.4.2 Physical Properties

The Υ (1S) is an hadron, more specifically a meson, composed of a bottom quark in a bound state with a bottom antiquark. Due to its heavy mass, it can be treated as a completely non-relativistic system [26]. The 1S denotes the fundamental state of a composite particle in spectroscopic notation [9]. As most bottomonium mesons, it can undergo a variety of transitions [27], which makes it a very versatile meson.

Upsilon Υ (1S)			
Composition	Charge	Spin	Experimental Mass (MeV)
$b\bar{b}$	0	1	9460.30$\pm$26

Table 1.5: The physical properties of the Υ (1S) meson [25] [27] [28]

Note that the mass shown in table 1.5 is the *experimental* mass. The theoretical mass varies depending on how the potential is defined, as equation 1.5 is just one of the many models physicists use for these mesons [27].

1.4.3 Detection

Due to their short life-spans, around $1.21x10^{-20}$s, ϒ mesons are not directly measured; they are instead *back-traced* measured through their decays into other particles. While the ϒ (1S) meson has many decay modes[29], in this work it was measured through one of its leptonic decays , the di-muon decay. The reason behind this is that, unlike hadronic decays, leptonic processes are electromagnetic, so they don't generate as much noise as their QCD counterparts.

Upsilon ϒ (1S) Leptonic Decay Modes	
Mode	Fraction Γ_i/Γ
$\tau^+\tau^-$	$(2.60 \pm 0.10)\%$
e^+e^-	$(2.38 \pm 0.11)\%$
$\mu^+\mu^-$	$(2.48 \pm 0.0.5)\%$

Table 1.6: Leptonic decay modes of the ϒ (1S) meson [29]

The di-muon decay was selected over the tau and electron decay for two different reasons: regarding the tau decay, as the tau is a rather unstable particle, we would not be able to measure it directly, but instead back-trace it through it decays, which would make the analysis considerably more complex; regarding the electron decay, the CMS can't properly identify them, imposing an experimental limitation for this process.

Figure 1.4: Feynman diagram of the botommonium decay into muons [30]. Note that, as the process is electromagnetic, the mediator particle is a photon.

The muons are reconstructed using information from the detector chambers, and the events that contain two well-matched muon tracks that fill the criteria are identified as ϒ (1S) events [31]. The detector components will be explained in chapter 2, and the criteria in question will be explained in detail in chapter 3.

1.4.3.1 Probing Qualities

The Υ (1S) has been shown to be a useful probing method for various physical phenomena. It has even been used as a probing mechanism for dark matter [32] [33]. In particle physics, the Υ (1S), and quarkonia in general, is used as a probing mechanism for an state of matter known as Quark-Gluon Plasma (QGP) [19] [20] [21] [34], a state of matter in which quarks and gluons are free of the strong force effects due to being under extremely high energy densities [35].

The Υ serves then as an exterior probing mechanism of QGP because of its relatively larger than the hadronic scale binding energy ($1.2GeV$ versus $0.2GeV$), and as a consequence of this they are much more smaller; also, since they have a relatively long lifetime compared to QGP, they can survive in QGP long enough for them to escape to decay into muons and be measured by the detector. This detection allows particle physicists to see if QGP was actually produced and to better understand its properties [19] [35].

CHAPTER 2
Experimental Facilities

Experimental particle physics has made much progress since the beginning of the 20^{th} century: from the discovery of X-rays to present day modern accelerators, the advancement in technology has allowed the study of particles at much higher energies than ever before [36]. The present chapter will focus solely on the biggest and highest energy accelerator built to date: the CERN's **L**arge **H**adron **C**ollider (**LHC**), and one of the main experiments held by the collider, the **C**ompact **M**uon **S**olenoid (**CMS**). The data of this study was taken from a GEANT4 simulation of the CMS detector at energies of 5.02 TeV.

2.1 CERN and the LHC

CERN, from french ***C**onseil **E**uropéen pour la **R**echerche **N**ucléaire*, is the European Organization of Nuclear Research, founded in 1954. Located near Geneva on the Franco-Swiss border, it was originally formed by 12 member states; there are now 23 countries fully involved in the maintenance of the project [37]. The scientists and engineers at CERN are responsible for maintaining, operating and upgrading the LHC accelerator complex, as well as all the particle detectors that are housed at CERN [19].

Discussions to build a large particle accelerator that would enable researchers at CERN to create particle collisions at high energies go as far as 1976. After many failed projects and multiple redesigns, the goal was achieved in 2008 as the LHC [38].

The LHC is a two-ring-superconducting-hadron accelerator and collider installed in a 26.7km tunnel underground. It aims to reveal the physics beyond the Standard Model with centre of mass collision energies of up to $14 TeV$ [39]. It has two virtually independent magnetic channels, which allows for higher luminosity values, with updates to attain higher values currently undergoing [40].

There are four main experimental insertions at the LHC [19]:

- **A T**oroidal **L**arge LHC **A**pparatu**s** (**ATLAS**).
- **C**ompact **M**uon **S**olenoid (**CMS**).
- **A L**arge **H**adron **C**ollider **E**xperiment (**ALICE**).
- **L**arge **H**adron **C**ollider **b**eauty (**LHCb**).

The first two are high luminosity experiments using pp collisions; the third is a low luminosity experiment for ion collisions and the fourth is a one B-meson experiment requiring medium luminosities for pp collisions [40].

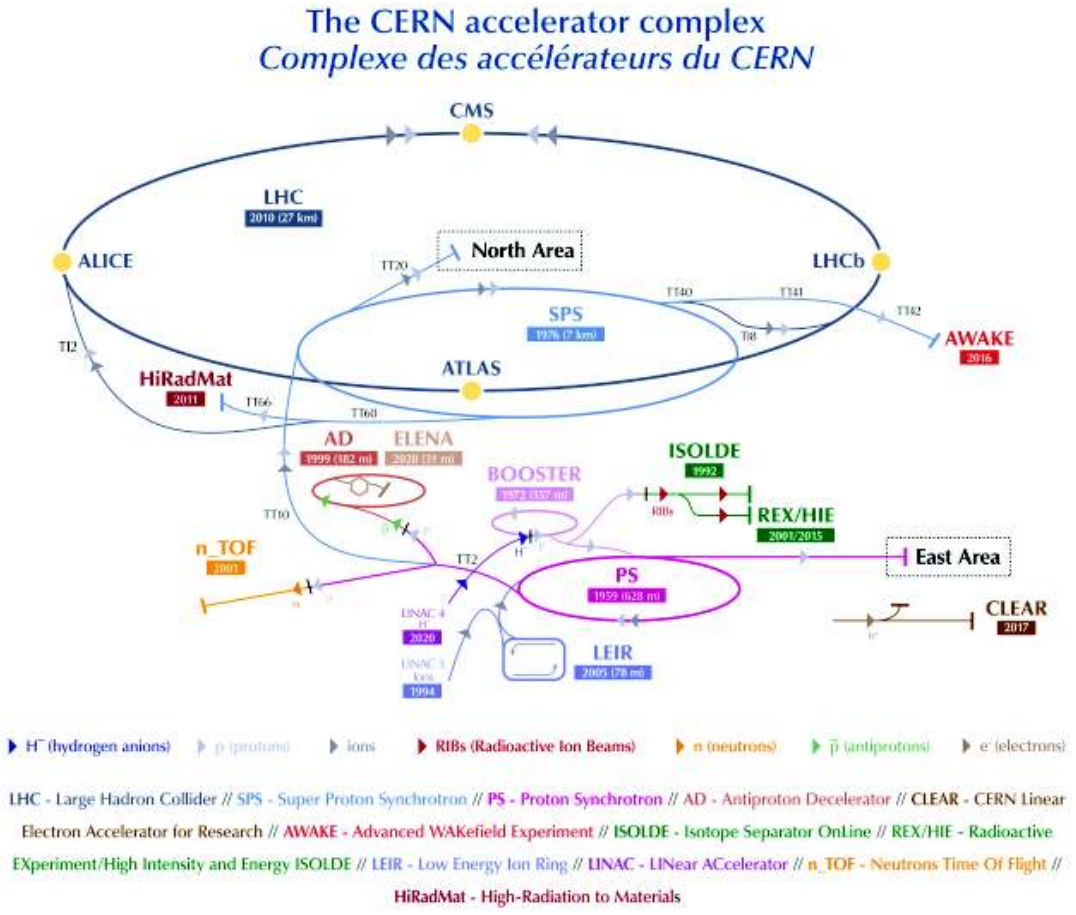

Figure 2.1: CERN accelerator complex [41].

2.2 Compact Muon Solenoid (CMS)

The CMS detector is a multi-purpose apparatus that operates at CERN's LHC, installed about 100 meters underground close to the village of Cessy, France [42].

2.2.1 History

The CMS as a concept was presented in October 1990, before the LHC was even approved, at the LHC workshop in Aachen. Years later, in 1992, at the Evian meeting there was a conceptual design of the complete detector was presented as an Expression of Interest by a 49 institutions collaboration. The design goals fo CMS were defined as follows [43]:

1. A very good and redundant muon system.
2. The best possible electromagnetic calorimeter (ECAL) consistent with 1.
3. A high quality central tracking to achieve 1 and 2.
4. A financially affordable detector.

At the time of the submission of the technical proposal in 1994 for the final design of the experiment, more than 132 institutions were involved in the project. Needless to say the proposal was accepted, and the CMS was built along the rest of the LHC accelerator complex and ran for the first time in 2008 [38].

2.2.2 Coordinate System

The CMS detector was designed under a right-handed cylindrical coordinate system: the origin is centered at the nominal collision point of the experiment, the x-axis pointing radially inward towards the center of the LHC, the y-axis pointing vertically upward and the z-axis pointing along the beam direction.

As is usual with cylindrical coordinates systems, the azimuthal angle ϕ is measured from the x-axis in the x-y plane, the radial coordinate in this plane is denoted by r, and the polar angle θ is measured from the z-axis.

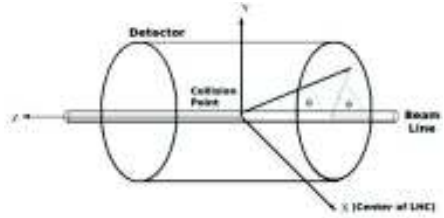

Figure 2.2: Coordinate system used by the CMS experiment [44].

The CMS experiment uses an additional coordinate to those of a regular cylindrical coordinate system, which is the *pseudorapidity* η, defined in relation to θ as

$$\eta \equiv -ln\left[tan\left(\frac{\theta}{2}\right)\right] \tag{2.1}$$

which allows the momentum and energy transverse momentum, p_T and E_T, to be computed from the x and y components [42]. The physical importance of this coordinate will be explained in section 2.2.3.1.

Another relevant geometrical variable in the CMS is the *rapidity* y, defined as [45]:

$$y \equiv \frac{1}{2}ln\frac{1+\frac{p}{E}cos\theta}{1-\frac{p}{E}cos\theta} \tag{2.2}$$

where E is the energy and p is the momentum of the particle. The physical importance of this coordinate will be explained in chapter 3.

2.2.3 Detector Components

The CMS is a 14500 tonnes detector with a diameter of 14.6m and an overall length of 28.7m [43]. Figure 2.3 shows an schematic view along with its labeled components.

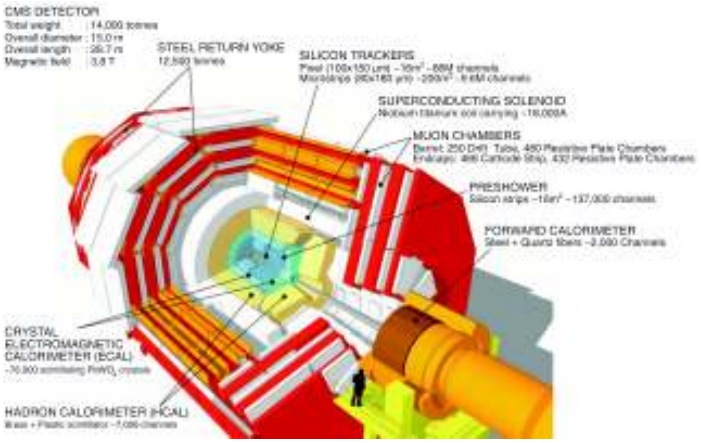

Figure 2.3: Schematic view of the CMS detector showing its main components [46].

The CMS detector consists of several cylindrical detection layers, nested around the beam axis. Each layer interacts with each particle in accord to their physical properties. Starting from the beam interaction region onwards, particles first enter a tracker: here, charged-particles trajectories, known as *tracks*, and their production location, known as *vertices*, are reconstructed from signals or *hits*. This tracker is immersed in a magnetic field that interacts with the charged-particles and bends their trajectories, thus allowing the measurement of their electric charges and momenta. The next layer is the electromagnetic calorimeter (ECAL), and is where electrons and photons are absorbed. These electrons and photons generate electromagnetic showers, detected as *clusters* of energy, which are then recorded in neighbouring cells and allows the determination of the energy and direction of such particles. Charged and neutral hadrons may initiate what is known an *hadronic shower*, in this layer; it will be subsequently fully absorbed in the next one, the hadron calorimeter (HCAL), where their corresponding clusters are used to estimate their energies and directions. Muons and neutrinos traverse these layers with little to no interactions. Later on, neutrinos escape mostly undetected, but in the outer tracking layers, known as muon detectors, muons produce hits that allows for their reconstructions. At the end of the process, the information measured goes through computational systems known as triggers, which chooses events based on a list of signatures set by the physicists at CMS for events deemed useful for the analysis [47]. Figure 2.3 graphically summarizes this explanation.

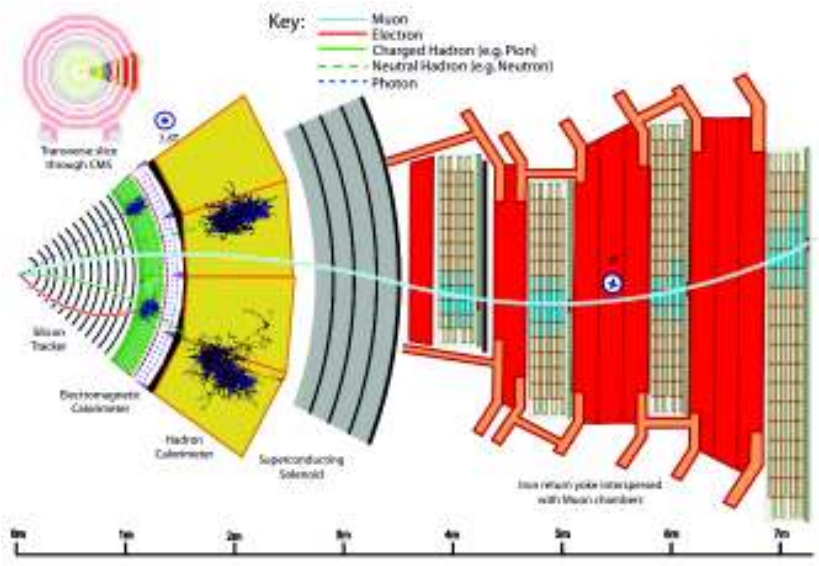

Figure 2.4: Transverse slice of the CMS detector [47]. Note that each particle interacts distinctly through the different layers, as explained above.

2.2.3.1 Tracker

The purpose of the inner tracking system is to provide a precise and efficient measurement of the trajectories of charged particles that emerge from the LHC collisions and a precise reconstruction of secondary vertices. It surrounds the interaction point over a diameter of $2.5m$ and a length of $5.8m$, and is under an homogeneous magnetic field of $4T$ coming from the CMS solenoid. The tracker itself is made of two a pixel detector and a silicon strip tracker: composed of 1440 pixel modules and 15148 strip detector modules, each serves different functions.

The first part of the tracker closest to the interacting region is the **pixel system**. It contributes precise tracking points in the $r-\phi$ plane and z, and as such it is an important factor for good vertex reconstructions.

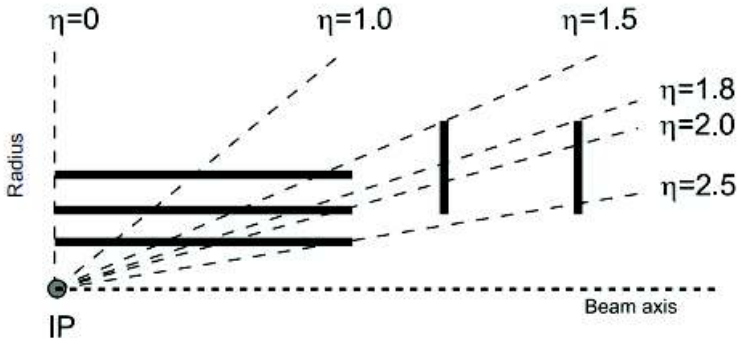

Figure 2.5: Geometrical layout of the pixel detector hit coverage [42]. As explained in section 2.2.2, η is a function of θ. The diagram is a bit outdated, as the tracker has now four layers.

As shown in figure 2.5, the pixel detector covers a pseudorapidity range of $-2.5 < \eta < 2.5$, which sets a crucial condition that will be revisited in chapter 3.

The second and outer part of the tracker is the **silicon strip tracker**. It serves as an analogical method to double-check the measurements from the pixel system, and as such, has the same hit coverage [42].

2.2.3.2 Electromagnetic Calorimeter (ECAL)

The ECAL is a hermetic homogeneous calorimeter made of lead tungstate $PbWO_4$ crystals [47]. These crystals work as scintillators, which emit blue-green lights proportional to the energy of the electrically charged particles interact through them. This calorimeter allows the detection of photons and electrons [42].

2.2.3.3 Hadronic Calorimeter (HCAL)

The HCAL is a hermetic sampling calorimeter that consists of several layers of brass absorber and plastic scintillator tiles [47]. Along with the ECAL, its mains task is to measure accurately the direction and energy of the particles and of the transverse energy flow. Each of these layers has is of a thickness proportional to the lifespan and interaction rate of hadrons, which allows their detection and measurement [48].

2.2.3.4 Superconducting Solenoid

Central feature of the CMS design, this large superconducting solenoid magnet delivers an axial and uniform magnetic field of approximately $4T$ over a length of $12.5m$ and a free-bore radius of $3.15m$, which is large enough to accommodate the tracker, the ECAL and the HCAL [47]. The conductor itself is made from a Rutherford-type cable co-extruded with pure aluminium, and is mechanically reinforced with an aluminium alloy [42].

2.2.3.5 Muon Chambers

The last layer, located outside the solenoid coil, is comprised of several muon detectors. In this layer, the magnetic flux is returned through a yoke consisting of three layers of steel interleaved with four muon detector planes [47]. Each of these four detector planes, or ”barrel” muon stations, consists of twelve planes of aluminium Drift Tubes (DTs) arranged in twelve azimuthal sectors in a way that there are no cracks pointing to the primary vertex, thus avoiding the possibility of any muon escaping undetected. Each station consists of sectors of Cathode Strip Chambers (CSC) overlapping to assure full coverage [43].

These chambers are complemented by a system of double-gap Resistive Plate Chambers (RPC), which consists of two parallel bakelite electrodes with a $2mm$ gas gap, placed on top of another with common copper readout strips in between using a three-component gas mixtures [49].

2.2.4 GEANT4 Simulation

Due to the magnitude of the data and the need to make sense of it and search for new physics, physicists at CMS have designed computer simulations of the LHC collisions and the CMS detector. There are currently two main types of simulations used by the CMS Collaboration: a detector model that uses simplified geometry, response evaluation and patter recognition to decrease the processing time per event, known as the ”fast” simulation [50], and a MonteCarlo based simulation, known as the ”full” simulation, which is based on the GEANT4 toolkit [51]. The data of the present work comes from the GEANT4 simulation software.

The simulation code is built like any CMS specific software package application, in the form of special shared object libraries known as ”plugins”, with the configuration files being written in python. The present work is based on the $9.4.p03$ version of GEANT4 which provides [52]:

1. The physics processes for electromagnetic and hadronic interactions.
2. Tools for building detector geometry and sensitive element response.
3. Interfaces for tuning and monitoring particle tracking.

2.2.4.1 Generated and Reconstructed Data

In GEANT4, we can differentiate between two sets of data: generated and reconstructed. **Generated** data is the one that was originated by the PP collision, from partonic dispersion and particle hadronization, to the subsequent particle decays. **Reconstructed** data refers to all the physical processes that follow the particle travel through the detector, that is, it ”reconstructs” the physical interactions of the particles with the detector components.

2.2.4.2 Generator: PYTHIA 8

To generate the events, the simulation used PYTHIA 8 as a generator. PYTHIA is a program for the generation of high-energy physics events, that is, for the description of collisions at high energies between electrons, protons, photons, and heavy ions, categorized as a ”general purpose Monte Carlo event generator” [53].

In this particular simulation, the principal production source of bottomonium is through the fusion of gluons, which in turns generates a $b\bar{b}$ pair that then hadronizes following the NRQCD (Non-Relativistic QCD) process. This bottomonium production can be of either the base state Upsilon (1S), as well as the other excited states such as the Upsilon (2S) and Upsilon (3S); it can even produce η_b and χ_b mesons, also bound states of $b\bar{b}$, which then decay into the base state. Once the Upsilon (1S) is generated, its decays are forced completely into the dimuon channel.

CHAPTER 3

Acceptance and Efficiency Calculations

In all detector simulations, particle physicists must take into account a set of both physical and geometrical conditions both of the detector and the simulation itself. These set of conditions are what particle physicists know as ***Acceptance*** and ***Efficiency*** [54].

3.1 Experimental Variables

There are a set of experimental variables, besides η and y, one needs to understand to fully comprehend the conditions set by both acceptance and efficiency [45]:

- **Invariant mass**: mass m of a particle as measured in its rest frame [55] and is defined as [56]

$$m \equiv \sqrt{E^2 - p^2} \tag{3.1}$$

- **Transverse Momentum** p_T: momentum of a particle that is perpendicular to the beam direction as seen in figure 2.2. Measured in gigaelectron-volts (GeV), it is defined as

$$p_T^2 \equiv p_x^2 + p_y^2 = psin\phi \tag{3.2}$$

- **Transverse Energy** E_T: energy of a particle in the rest frame where $p_z = 0$. Measured in gigaelectron-volts (GeV), it is defined as

$$E_T \equiv E^2 - p_z^2 \tag{3.3}$$

3.2 ROOT

ROOT is a framework for data processing created at CERN. It is an object-oriented program and library built in C++ that allows the user to save, access and mine data, as well as publishing results via visual interfaces such as graphs or histograms, run or build self-made applications and use it within other languages, such as python and R.

The current version is ROOT *v*6.20/04 [57], which was the one used for the data analysis in this study, ran on an Ubuntu 18.04 virtual machine in a Windows 10 system. The following statistical procedures were done through ROOT codes ran in this system.

3.3 Acceptance and Efficiency

The results of the following procedures can be seen in chapter 4 as 1 one-dimensional histograms (the p_T spectrum) and two-dimensional histograms (the p_T vs η spectrum).

3.3.1 Acceptance

The acceptance of a detector refers to its purely geometric fiducial volume [54], that is, the geometrical conditions of the detector, and is defined as [58]

$$\alpha = \frac{N_{GEN}\left[|y^{\mu\mu}| < 2.4, |\eta^{\mu}| < 2.4, p_T^{\mu} > 3.5 GeV/c\right]}{N_{GEN}\left[|y^{\mu\mu} < 2.4\right]} \tag{3.4}$$

which reads as the number of generated Upsilon particles whose absolute value of rapidity y is less than 2.4, and whose individual muons η absolute value is less than 2.4 and p_T is greater and $3.5 GeV/c$, over the number of generated Upsilon particles whose absolute value of rapidity y is less than 2.4. Note that while the acceptance refers to geometrical conditions, there is also a p_T cut; this is to filter out all of the muons that do not have the minimum p_T value to have come from an Upsilon (1S) particle.

The condition for η and y come from the physical limitations of the pixel tracker as explained in section 2.2.3.1; the reasons for the p_T conditions will not be explained in this work.

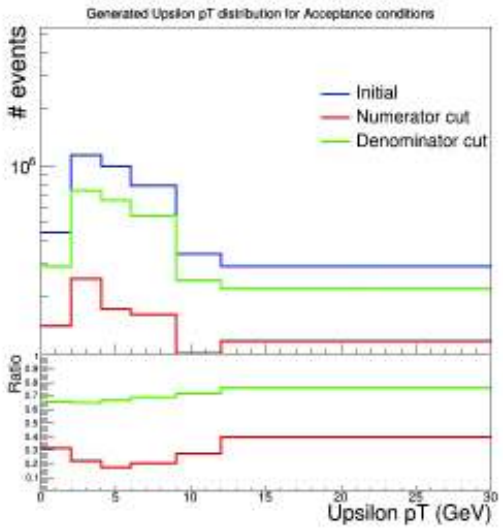

Figure 3.1: Distribution of the generated Upsilon p_T spectrum within fiducial region indicated in equation 3.4.

Figure 3.1 shows the change in events in the p_T spectrum after applying the conditions stated in equation 3.4. The numerator cut filters out much more events than the denominator cut; the effects in the latter are practically constant through the whole spectrum, as can be seen in the initial to cut ratio, while the former shows a greater effect for $p_T > 5$ GeV.

3.3.2 Efficiency

The efficiency of a detector refers to how effective a detector is to find objects that have passed through it [54], and is defined as [30]

$$\varepsilon = \frac{N_{RECO}\left[|y^{\mu\mu}| < 2.4, Acc(\mu^+,\mu^-), QualityCut(), 8.5 < m^{\mu\mu} < 11.0\right]}{N_{GEN}\left[|y^{\mu\mu}| < 2.4, Acc(\mu^+\mu^-)\right]} \tag{3.5}$$

where $Acc(\mu^+,\mu^-)$ are the acceptance conditions for the dimuons, $QualityCuts()$ are a series of individual conditions described on the next page, and $m^{\mu\mu}$ is the mass of the $\Upsilon(1S)$ particle. Equation 3.5 then reads as the number of reconstructed dimuons that pass the acceptance requirements for the dimuons, the quality cuts, and has Upsilon particlethat pass the rapidity and mass requirements, over the number of generated particles that pass the acceptance and the rapidity requirements for the dimuons and the Υ particles, respectively.

The $QualityCuts()$ are a series of muon matching, tracker, and kinematic requirements, defined as follows [59]:

- Acceptance conditions.
- $|y^{\mu\mu}| < 2.4$
- *isGlobalMu*: selects muons that have at least a matched track in both the muon station and the tracker.
- *isTrackerMu*: selects muons that have at least a match in the silicon tracker.
- $nTrkWMea > 5$: selects muons whose muon tracks have at least six silicon tracker hits. This supresses muons from decays in-flights.
- $nPixWMea > 0$: selects muons that have at least one silicon pixel hit. Guarantees a good p_T measurement and supression of in-flight decay muons.
- *Reconstructed Upsilon* $p_T < 100GeV$
- $8.5GeV <$*Reconstructed Upsilon m* $< 11.0GeV$
- *Opposite sign muon* ($\mu^+\mu^-$)
- $VtxProb > 0.1$: the probability that the oppositely charged muons comes from the same origin is greater than 10% [60].
- $HLT\_HIL1DoubleMu0\_v1$ *Trigger*: the event was selected by the corresponding trigger for the dimuon decay channel.
- $dxy < 0.3cm$: selects muons whose distance of the muon track from the closest primary vertex is less that $3mm$ in the transverse direction.
- $dz < 20cm$: selects muons whose distance of the muon track from the closest primary vertex must be less than $20cm$ in the longitudinal direction.

The last two are geometrical requirements guarantee that the two muons come from a vertex close to the interaction point, which means that their origin particle decayed relatively fast, that is, has a short lifetime, a quality of the $\Upsilon(1S)$.

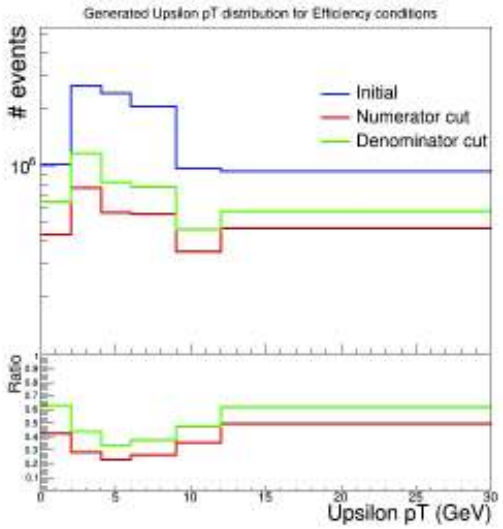

Figure 3.2: Distribution of the generated Upsilon p_T spectrum within fiducial region indicated in equation 3.5.

Figure 3.2 shows the change in events in the p_T spectrum after applying the conditions stated in equation 3.5. The difference in filtered events is not as wide as the one shown in figure 3.1, and the initial to cuts ratio shows a similar evolution in p_T values for both cuts.

3.3.3 Acceptance times Efficiency

To correctly calculate the actual number of acceptable events out of a measurement, one must apply both acceptance and efficiency to the real world data. In one-dimension, this is done through a multiplication of the two quantities; for two-dimensions, this was done through the multiplication of the individual bin value of each histogram, event by event. This results in an *Acceptance times Efficiency* ratio that allows physicists to see the true number of events measured by the detector, which in 1-dimensions is seen as an histogram and in 2-dimensions is seen as individual, correction values.

3.4 Raw Yields Fit

The next part of the statistical analysis consisted in finding the relationship between the simulation data and real world data. This was done through a process known as *raw yield fitting*.

Essentially, the **raw yields** are the number of Upsilon (1S) particles that were produced through the invariant mass fits [30].

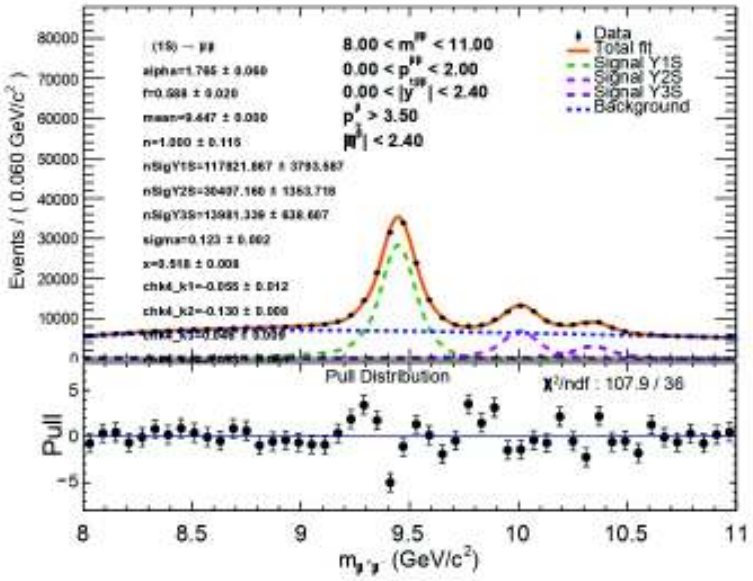

Figure 3.3: Invariant mass fit of Upsilon (1S). The number of particles produced are the raw yields [30].

The process comprised the following steps:

1. Correct the raw yields by Acceptance times Efficiency.
2. Divide each bin by their respective bin width.
3. Normalize the resulting histogram by dividing each bin over the sum of all of the bins content.
4. Divide the normalized histogram over the Acceptance denominator.

This serves to show how our simulation relates to the ”real” data used by the detector.

3.4.1 Raw Yields Fit: the weight function

To fit the resulting raw yields calculations, the following function was used

$$f(x) = \frac{A + Bx + Cx^2}{(x - D)^3} \tag{3.6}$$

with the parameters values set as

$$A = 251.102$$

$$B = 18.5373$$

$$C = 23.5803$$

$$D = -4.97668$$

The function and the parameters values were provided beforehand [30].

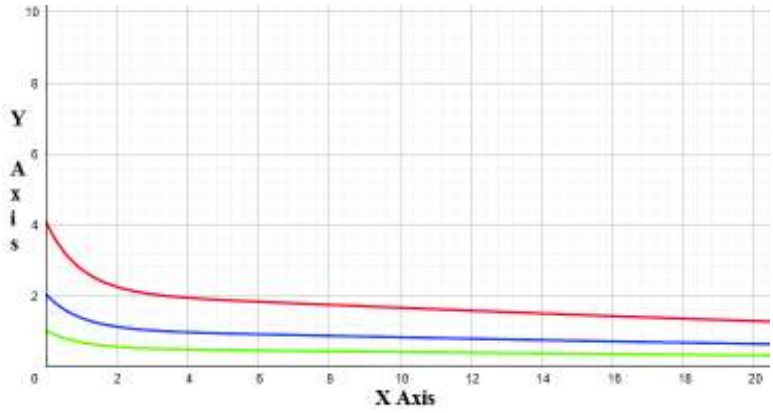

Figure 3.4: Graphic of the weight function shown in equation 3.6 for both the normal and amplified weight effects, using GeoGebra [61]. The axis are merely numerical values and have no physical significance.

Figure 3.4 shows the function values for three different cases: the blue line shows the normal function values, the red line shows the function values multiplied by a factor of 2 and the green line shows the function values multiplied by a factor of $\frac{1}{2}$; these are all cases that will be used when applying weights.

Following this fit, this function proceeded to be defined as the **weight function** of the analysis.

3.5 Fine Binning

During the calculations, the goal was to obtain the finest possible bining while maintaining statistical consistency for the Upsilon p_T distribution. The problem that arised is that, to be able to do that, one needs two probabilistically independent samples, as the statistical methods that check for statistical consistency need at least two to verify it, while there was only 1 sample available. As a solution to this issue, the odd and even events were separated as two different, thus probabilistically independent, samples.

The fine binning process was done as follows for both Acceptance and Efficiency. This analysis was done for 1 dimension (the p_T spectrum) and 2 dimension (the p_T vs η spectrum) alike.

3.5.1 1-Dimensional Fine Binning

The following process was done using the 1 Dimensional p_T spectrum of both the Acceptance and Efficiency events from their corresponding root files:

1. Calculate Acceptance and Efficiency on even events (correction sample).
2. Correct the odd events Acceptance and Efficiency numerator (test sample) by dividing it over the correction sample.
3. Divide the corrected test sample over the odd Acceptance/Efficiency denominator.

In practice, by doing the previous steps, what is actually being done is

$$\frac{\frac{Numerator_{odd}}{\frac{Numerator_{even}}{Denominator_{even}}}}{Denominator_{odd}} = \frac{\frac{(Numerator_{odd})(Denominator_{even})}{Numerator_{even}}}{Denominator_{odd}} \approx \frac{Denominator_{even}}{Denominator_{odd}}$$

Since the samples come from the same simulation, their resulting number of events should be almost the same for the same cuts; as such for statistically consistent bins, approximates as

$$\frac{Denominator_{even}}{Denominator_{odd}} \approx 1 \tag{3.7}$$

The bins width is reduced multiple times until the approximation 3.7 no longer holds, as that means that the bins are no longer statistically consistent.

3.5.1.1 Weighted 1-Dimensional Fine Binning

The one-dimensional fine binning process was repeated a second time using the weight function to calculate the weight values of both the even and odd Acceptance and Efficiency, as a way to check if the fit used was a proper weight function. The corresponding results are shown and explained in chapter 4.

3.5.2 2-Dimensional Fine Binning

While similar to its one-dimensional counterpart, the 2-Dimensional Fine Binning process has several differences that makes this process more statistically reliable, the key difference being that the histograms used as correction samples are the 2-Dimensional, p_T vs. η spectrum's.

The following process was done using the 2 Dimensional p_T vs. η spectrum's of both the Acceptance and Efficiency events from their corresponding root files:

1. Calculate Acceptance and Efficiency in 2-Dimensional p_T vs. η histograms on even events (correction sample).

2. Correct the odd events 2-Dimensional Acceptance and Efficiency (test sample), event by event, bin by bin, by using the Acceptance or Efficiency corresponding bin value as weights.

3. Divide the corrected test sample over the odd Acceptance and Efficiency denominator.

Unlike the one-dimensional process, in the 2-D analysis the bins only change in the correction sample; the bins in the test sample stay the same. Taking this into account as well as the fact that this correction is done individually event by event, bin by bin, makes this processmore statistically reliable because each bin has its own, precalculated weight, and thus does not depend on any fitted weight function.

3.5.2.1 Weighted 2-Dimensional Fine Binning

The 2-Dimensional weighted fine binning process is quite more complex than its 1-Dimensional counterpart, although it still serves the same key purpose: to verify the reliability of our obtained bins as well of our selected weight functions.

The following process was done using the 2 Dimensional p_T vs. η spectrum's of both the Acceptance and Efficiency events from their corresponding root files:

1. Calculate Acceptance and Efficiency in 2D without applying weights.
2. Calculate Acceptance and Efficiency in 2D applying weights.
3. Correct the Efficiency numerator using Acceptance times Efficiency values (without weights applied) from the corresponding bins as weights.
4. Correct the Efficiency numerator using Acceptance times Efficiency values (with weights applied) from the corresponding bins as weights.
5. Divide step 4 results over step 3 results.

As a way to verify our procedure, the weights effects were amplified in two different runs: once by a factor of 2, and then by a factor of $\frac{1}{2}$. The results were the same.

3.6 Systematic Errors

During a computational simulation, there are a series of physical and computational factors that cannot be simulated, variations carried by the same measurement devices we use and simulate. As they cannot be simulated, the simulation holds an ”error” when compared to the real values. This type of error is known as **systematic errors**, also known as *systematic uncertainties*.

There are a great variety of methods used to calculate these systematic errors. In this study, they were calculated using a statistical analysis known as *Tag and Probe method*, which, in essence, consists of using two data samples which differ only in the particle identification conditions; at least one of them has to fulfill the physical conditions for it to be a plausible candidate [62].

For the present work, the systematic error values were provided beforehand [63]. The errors values applied to the simulation take into the account the errors for each muon that surged by using the quality cuts for efficiency and the use of the simulated trackers, as explained in section 3.3.2.

Two types of error factors were used for the corrections in this work. The first is the **Global Muon Tight Acceptance**, which takes into account the associated error that emerged when applying the *isGlobalMuon* condition on our simulated data; the second condition is the **Hybrid Soft ID Trigger Tight Acceptance**, which corrects for the associated error that emerged when applying the trigger conditions to our simulated data.

Each error factor has three types of errors:

- Central Value (CtrlVal).
- Systematic Error (SystErr).
- Statistical Error (StatErr).

Each of these type of errors have one associated value for each muon for each error factors; that is, one associated value for the positive muon, and another different, independent associated value for the positive muon for each of the error factors, giving a total of four possible values for each type of error.

First, the nominal error correction was calculated as a multiplication of the central value of the two muons. As each muon has two associated central values, one for each correction, the nominal error value is the multiplication of the four associated central values.

Then, for each error factor, four additional error corrections were calculated, by adding and subtracting the associated systematic and statistical error, respectively, giving a total of nine error corrections.

CHAPTER 4
Analysis Results

In this chapter, the results of each statistical analysis is shown, as well as the corresponding statistical interpretation.

4.1 Acceptance and Efficiency Results

The one-dimensional histograms use a p_T binning, measured in GeV, of

$$p_{T_{bins}} = [0.0, 2.0, 4.0, 6.0, 9.0, 12.0, 30.0] \tag{4.1}$$

The two-dimensional histograms have a η binning that covers the range $-2.4 < \eta < 2.4$ in values of 0.2 ($-2.4, 2.2, 2.0, ...$), which derives from the pixel detector hit coverage explained in section 2.2.3.1.

The p_T binning used is the one obtained through the two-dimensional fine binning process, which resulted in

$$p_{T_{finebins}} = [0.0, 0.5, 1.0, 1.5, 2.0, 2.5, 3.0, 3.5, 4.0, 4.5, 5.0, 5.5, 6.0,$$

$$6.75, 7.5, 8.25, 9.0, 9.75, 10.5, 11.25, 12.0, 16.5, 21.0, 25.5, 30.0, 35.0, 40.0, 45.0, 50.0] \tag{4.2}$$

4.1.1 Acceptance Results

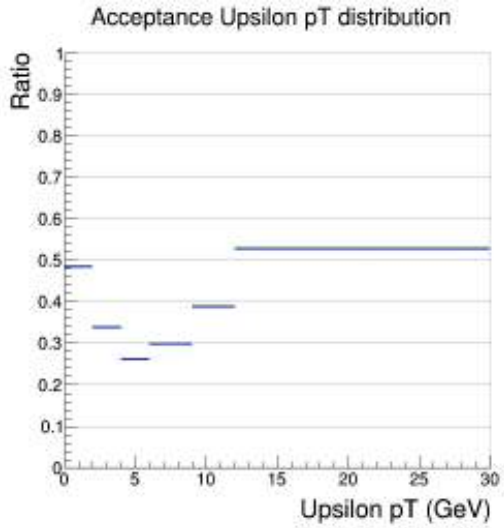

Figure 4.1: Acceptance Upsilon p_T spectrum in 1 dimension.

From the histogram, it can be seen that for low p_T values, between 0 and 12, the Acceptance ratio is less than 50%, which means that more than half the Υ(1S) measured by the simulation were lost.

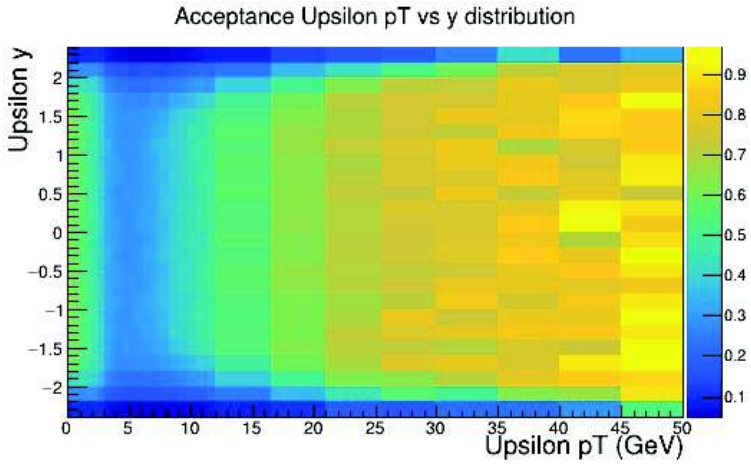

Figure 4.2: Acceptance in 2 dimensions, Upsilon p_T vs y spectrum.

The 2-Dimensional histogram shows a more complete view of the Acceptance ratio of the detector: it can be seen that the Acceptance ratio is higher as the pT increases, and it is also shown that at the edges the Acceptance lowers drastically, which helps visualize the geometrical limitations of the detector.

4.1.2 Efficiency Results

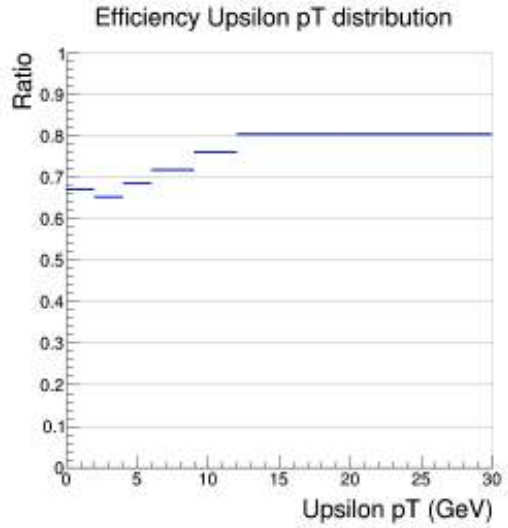

Figure 4.3: Efficiency Upsilon p_T spectrum in 1 dimension.

The Efficiency histogram shows a high acceptance ratio of the Υ(1S) measurements, with almost all of the spectrum the acceptance ratio close to 70%.

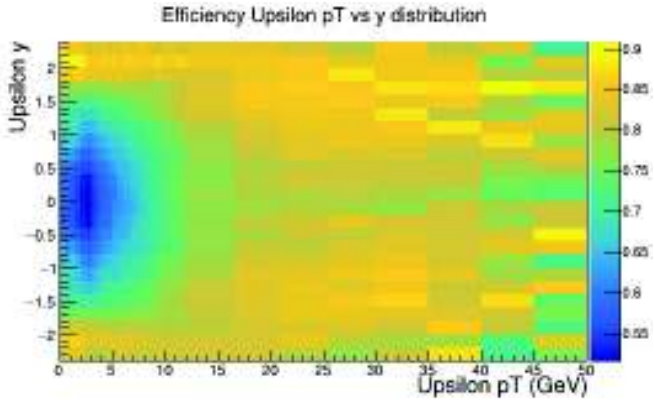

Figure 4.4: Efficiency in 2 dimensions, Upsilon p_T vs y spectrum.

The 2-Dimensional Efficiency histogram shows again that the efficiency ratio is much higher, even at high y values; as it is close to 1 at almost all y values for $p_T > 12$.

4.1.3 Acceptance times Efficiency Results

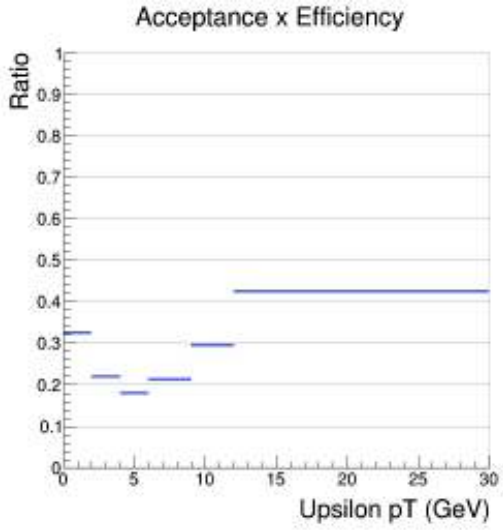

Figure 4.5: Acceptance times Efficiency Upsilon p_T spectrum in 1 dimension.

The Acceptance times Efficiency p_T spectrum shows, as expected from the individual Acceptance and Efficiency results, a lesser than 50% acceptance ratio overall.

4.2 Raw Yields Fit Results

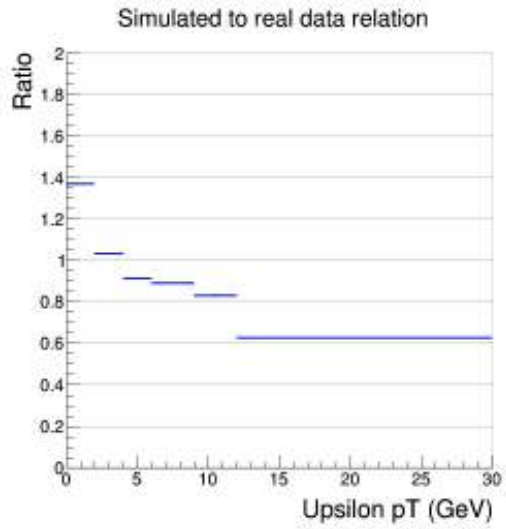

Figure 4.6: Simulated data to real data relation, Upsilonp_T spectrum.

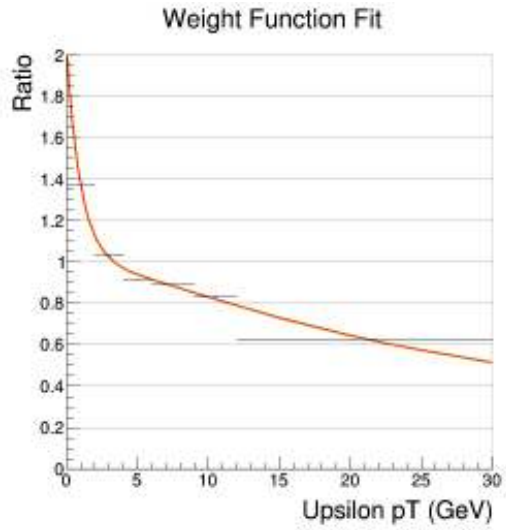

Figure 4.7: Upsilon p_T spectrum forthe weight function 3.6 fit.

Figure 4.6 shows the relation between our simulated data and the real data; it can be seen that our data begins with more events for low p_T values, progressively going lower as p_T increases. Figure 4.7 shows how our weight function fitted the ratio, following its down trend correctly; as such, it can be seen that our weight function can correct the discrepancies existing between our simulated data an real data.

4.3 Fine Binning Results

4.3.1 1-Dimensional Results

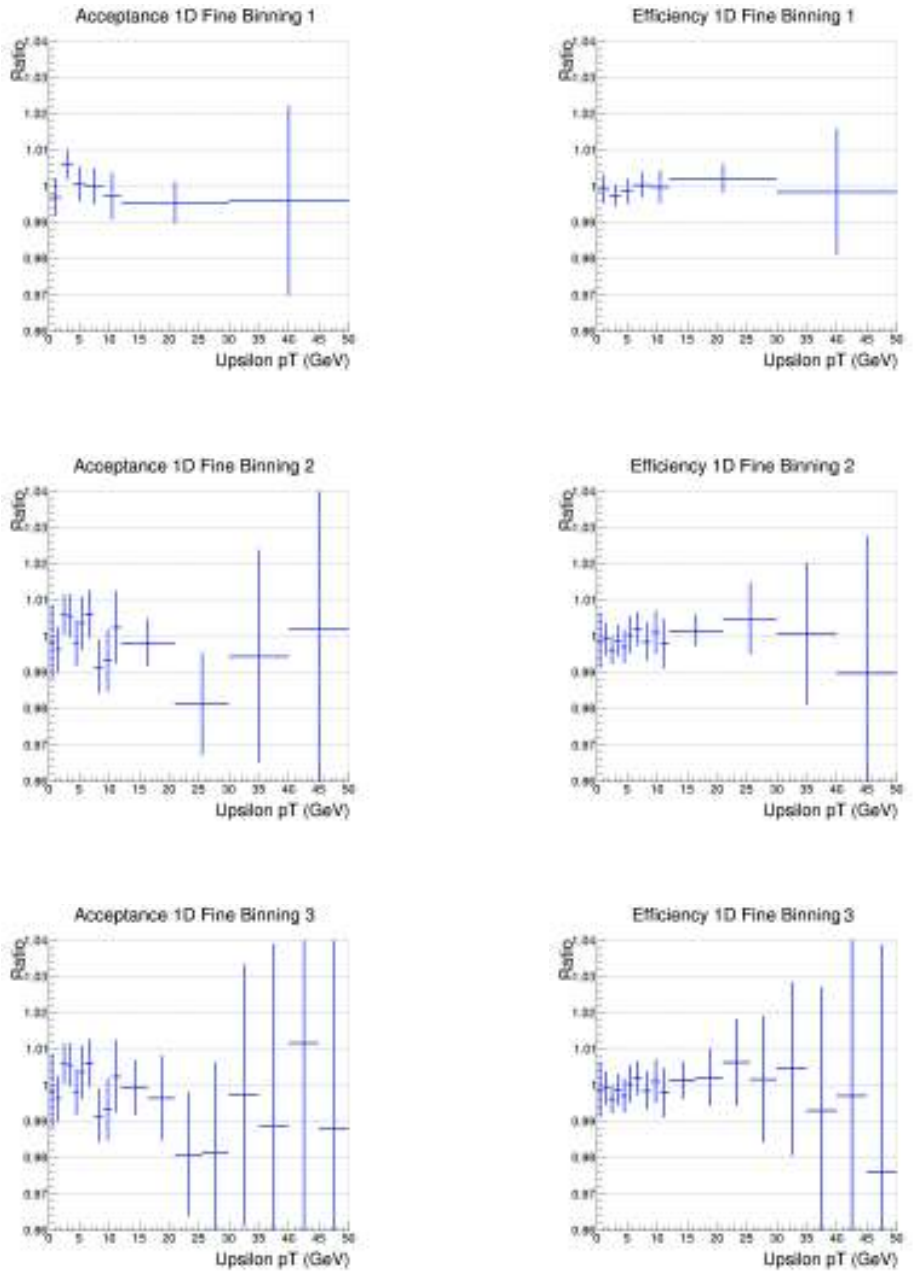

Figure 4.8: One-dimensional fine binning progressive results for Acceptance (left) and Efficiency (right).

The results from the 1-dimensional fine binning process shows how the odd and even events go from an almost 1:1 ratio to a visible statistical disruption, which indicates that the bins are at their statistical extreme and that our ”fine” bins were found.

4.3.1.1 1-Dimensional Weighted Results

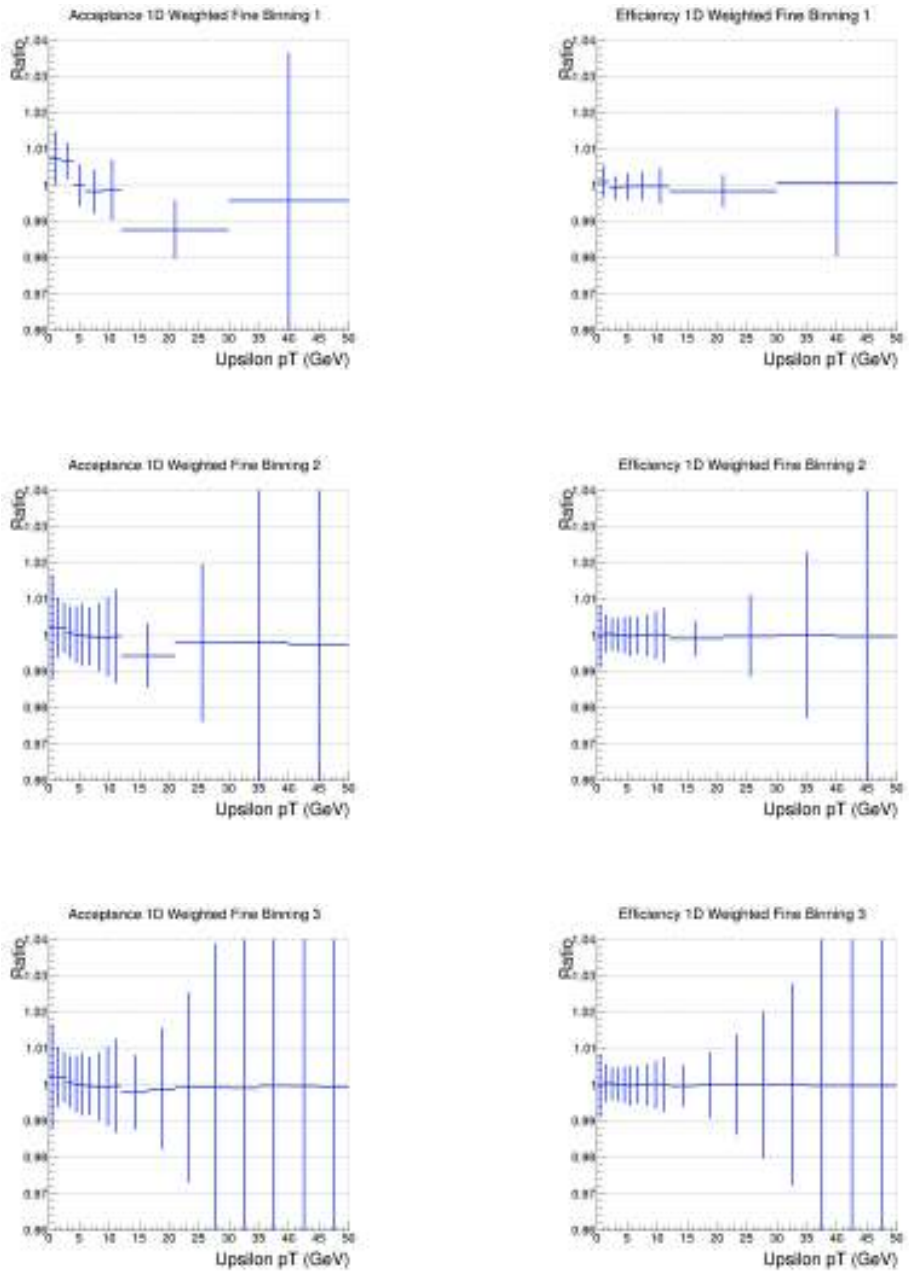

Figure 4.9: One-dimensional fine binning progressive results after applying the corresponding weights for Acceptance (left) and Efficiency (right).

The results from the 1-dimensional *weighted* fine binning process shows that the weight function with their set parameters is an statistically adequate weight function, as it can be seen from the last two graphics that the weight function ”fixes” the statistical disruption shown from the fine binning process, turning it to an almost ideal 1:1 ratio.

4.3.2 2-Dimensional Results

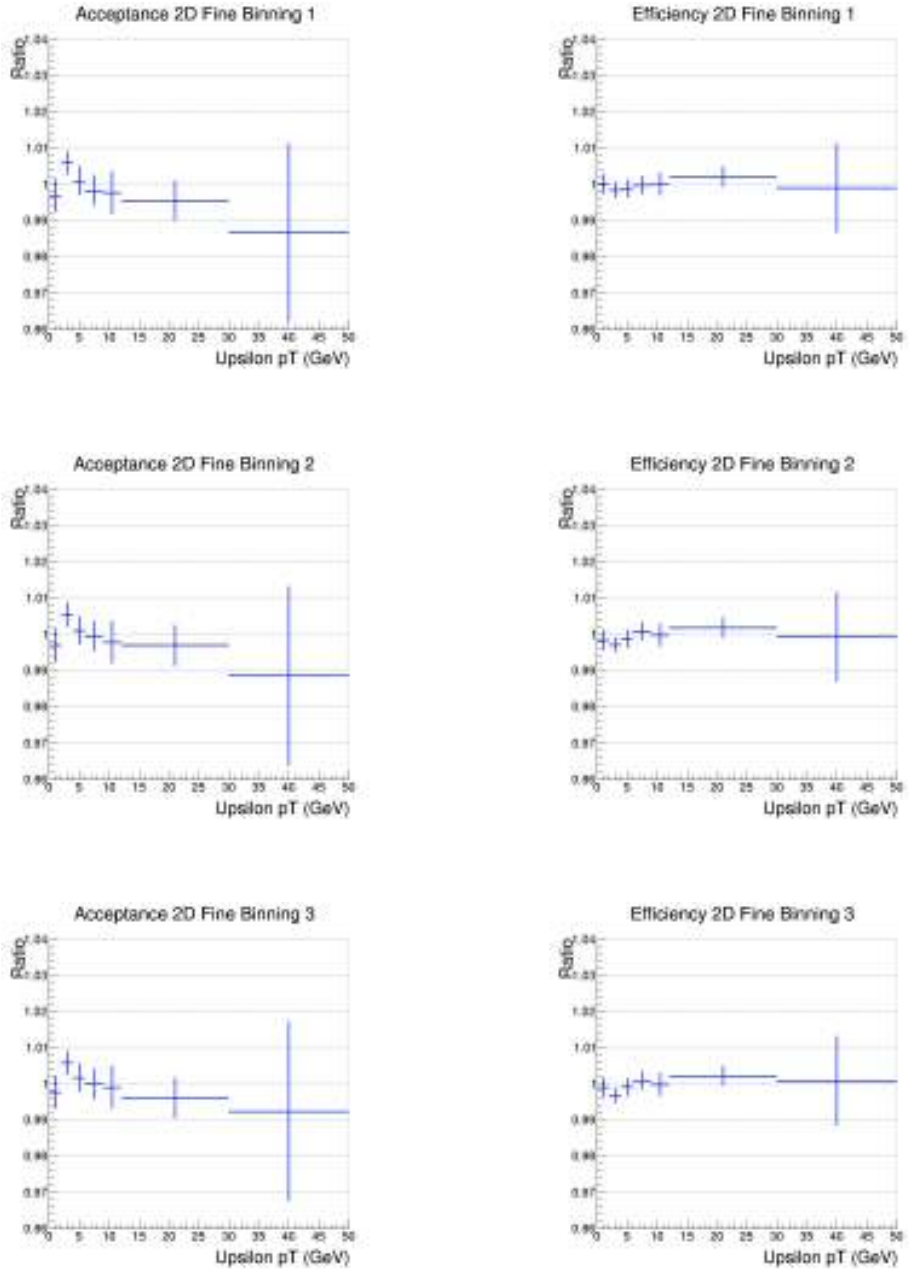

Figure 4.10: Two-dimensional fine binning progressive results.

The results from the 2-dimensional fine binning process shows that the 2D correction sample doesn't show as much statistical uncertainty as its 1-dimensional counterpart, but it's still noticeable enough for a visible statistical disruption. The final obtained 2D binning was similar to that shown in equation 4.2, but with each of the bins for values $p_T < 30GeV$ cut in half 2 times.

4.3.2.1 2-Dimensional Weighted Results

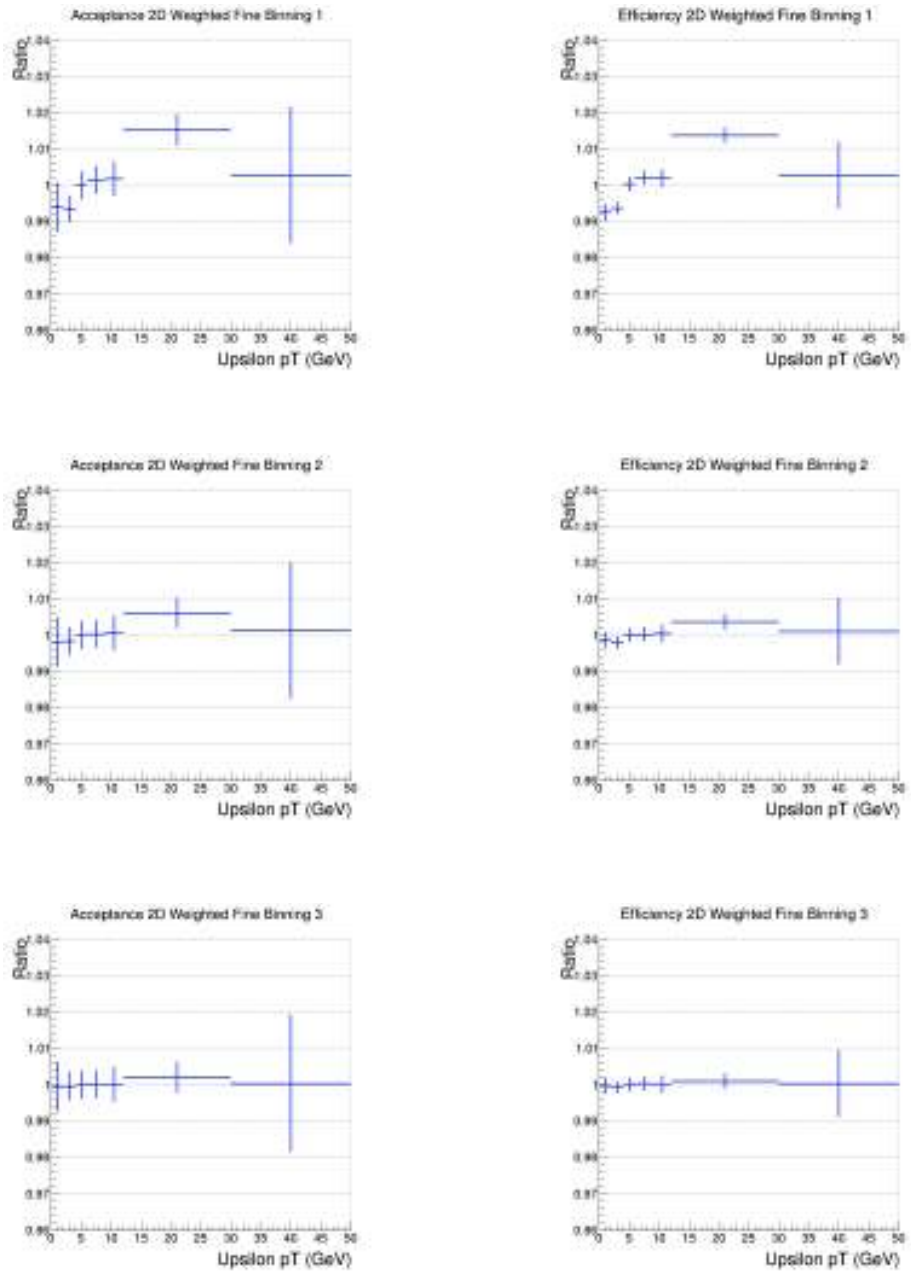

Figure 4.11: Two-dimensional fine binning progressive results after applying the corresponding weights for Acceptance (left) and Efficiency (right).

The 2-dimensional weighted fine binning results shows that what statistical uncertainty was present practically disappears as the bins get finer as a result of the Acceptance times Efficiency correction. From these results it can be said that the resulting bins are so fine that the correction is minimum, which is shown by the fact that the resulting quotient is practically 1.

4.4 Systematic Errors Results

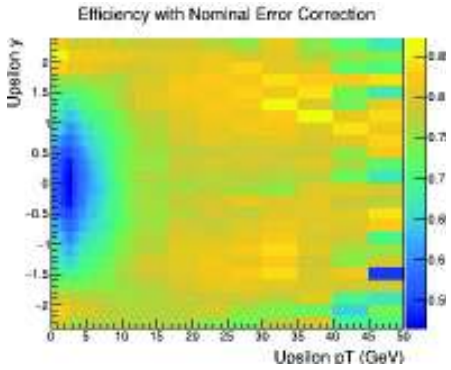

Figure 4.12: Efficiency spectrum using the nominal error correction.

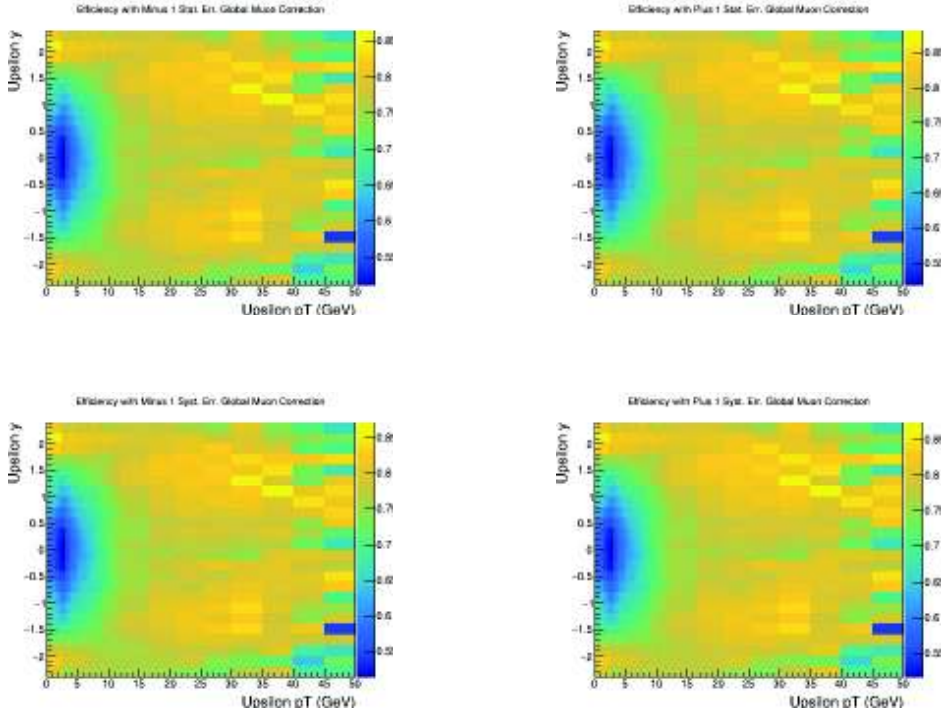

Figure 4.13: Efficiency spectrums using the Global Muons error corrections.

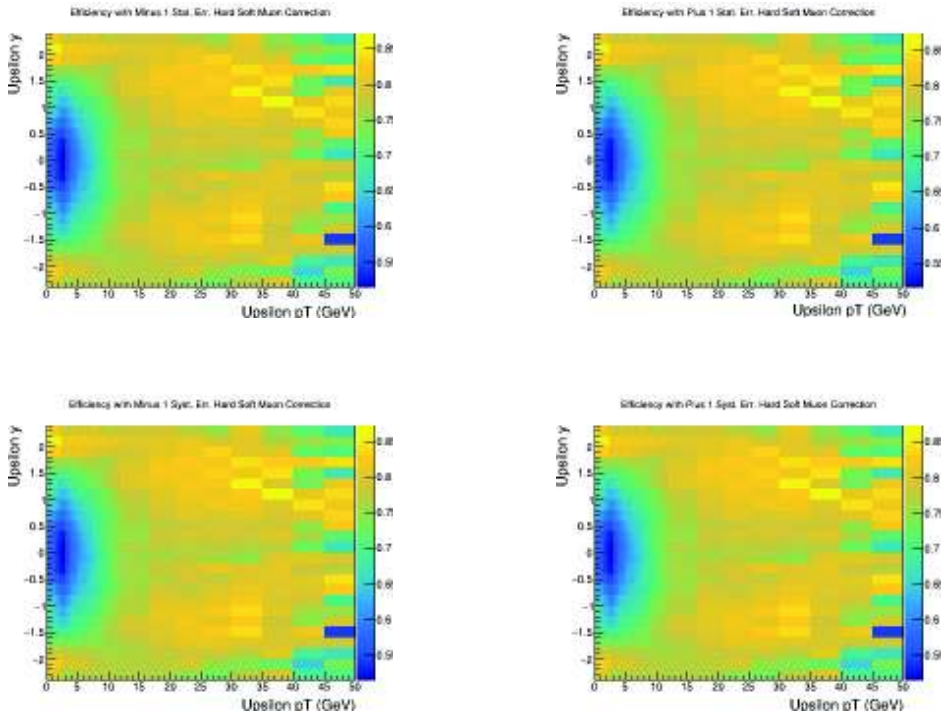

Figure 4.14: Efficiency spectrums using the Hard Soft Muon error corrections.

The various efficiency spectrum corrections show minimal differences that, while they are not obviously noticeable, have to be taken into account when applying the Efficiency correction ratios for our data, as these minimal differences can carry significant discrepancies between simulation and real data.

CHAPTER 5
Conclusions

The present thesis has presented a concise but complete framework for the calculations of Acceptance and Efficiency for the detection of Upsilon(1S) particles in a GEANT4 simulations of the CMS detector for pp collisions at 5.02 TeV. From the methods applied and the final histogram obtained, two final conclusions were obtained:

- The final Upsilon pT binning chosen for both Acceptance and Efficiency guarantees both maximal accuracy and statistical consistency, as was shown by the statistical methods applied.
- The final Acceptance and Efficiency two-dimensional histograms both show a higher ratio for $pT > 12$, meaning that the simulation results have to be taken cautiously for lower pT values.

5.1 Further Work

As it was mentioned earlier in this work, this thesis was but a small part of a bigger, more complete study being done by a group of scientists at the CMS experiment, expected to be published as an Analysis Note in 2022. As such, there is still a lot of work to be done: the Acceptance and Efficiency corrections calculated need to be applied to the actual data, after which more statistical analysis and work is to be applied. However, regarding the Acceptance and Efficiency calculations for this study in particular, no further analysis is needed.

Bibliography

[1] B. Russell. *History of Western Philosophy*. New York, New York, USA: Simon & Schuster, Inc., 1945.

[2] M. R. Kibler. "From the Mendeleev periodic table to particle physics and back to the periodic table". In: *Foundations of Chemistry* 9 (2007), pp. 221–234.

[3] K. S. Krane. *Modern Physics*. 4th ed. Hoboken, New Jersey, USA: John Wiley & Sons Inc, 2020. ISBN: 9781119495468.

[4] M. Thomson. *Modern Particle Physics*. New York, New York, USA: Cambridge University Press, 2013. ISBN: 9781107034266.

[5] D. Griffiths. *Introduction to Elementary Particles*. 2nd ed. Weinheim, BW, Germany: WILEY-VCH Verlag GmbH & Co., 2008. ISBN: 9783527406012.

[6] F. Halzen & A. Martin. *Quarks and Leptons: An Introductory Course in Modern Particle Physics*. Hoboken, New Jersey, USA: John Wiley & Sons Inc., 1998. ISBN: 0471887412.

[7] A. Bettini. *Introduction to Elementary Particle Physics*. 2nd ed. New York, New York, USA: Cambridge University Press, 2014. ISBN: 9781107050402.

[8] M. Veltman. *Facts and mysteries in Elementary Particle Physics*. 2nd ed. NToh Tuck Link, Singapore: World Scientific, 2003. ISBN: 9812381481.

[9] B. Martin & G. Shaw. *Paritlce Physics*. 3rd ed. Hoboken, New Jersey, USA: John Wiley & Sons Inc., 2008. ISBN: 9780470032930.

[10] J. Houston & F. Krauss J. Capmbell. *The Black Book of Quantum Chromodynamics*. New York, New York, USA: Cambridge University Press, 2018. ISBN: 9780199652747.

[11] D. M. Gingrich. *Practical Quantum Electrodynamics*. Boca Raton, Florida, USA: Taylor & Francis Group LLC, 2006. ISBN: 9781584885429.

[12] E. A. Paschos. *Electroweak Theory*. New York, New York, USA: Cambridge University Press, 2007. ISBN: 9780511273971.

[13] C. Y. Wong. *Introduction to High Energy Heavy-ion Collisions*. NToh Tuck Link, Singapore: World Scientific, 1994. ISBN: 9810202636.

[14] B. Povh et al. *Particle and Nuclei: An introduction to the Physical Concepts*. 7th ed. Berlin, Germany: Springer-Verlag, 2015. ISBN: 9783662463208.

[15] B. V. Vasiliev. "Some Problems of Elementary Particles Physics and Gilbert's Postulate". In: *Modern Physics* 7 (2016), pp. 1874–1888.

[16] J. Rojo. *Lecture 5: The QCD parton model, Deep-Inelastic scattering and Parton Distribution Functions*. Available at `https://www2.physics.ox.ac.uk/sites/default/files/2014-03-31/qcdcourse_juanrojo_tt2014_lect5_pdf_13977.pdf` (19/08/2021).

[17] X. Zhang. "Study of Heavy Flavours from Muons Measured with the ALICE Detector in Proton-Proton and Heavy-Ion Collisions at the CERN-LHC". PhD thesis. Clermont-Fernand, Auvergne, France, 2012.

[18] D. Griffiths. *Introduction to Quantum Mechanics*. 2nd ed. Upper Saddle River, New Jersey, USA: Pearson Education, Inc., 2005. ISBN: 0131911759.

[19] S. Tuli. "Quark Gluon Plasma and Cold Nuclear Matter modification of Υ stats at $\sqrt{s_{NN}} = 5.02$ TeV with the CMS Detector". PhD thesis. Davis, California, USA, 2019.

[20] N. Filipovic. "Measurement of Upsilon meson suppresion in heavy ion collisions with the CMS experiment at the LHC". PhD thesis. Paris, France, 2015.

[21] V. Knünz. "Measurement of Quarkonium Polarization to Probe QCD at the LHC". PhD thesis. Vienna, Austria, 2015.

[22] J. Domenech-Garret & M. Sanchis-Lozano. "QQ-onia package: a numerical solution to the Schrödinger radial equation for heavy quarkonium". In: *Computer Physics Communications* 180 (2009), pp. 768–778.

[23] R. Kumar & F. Chand. "Series solutions to the N-dimensional radial Schrödinger equation for the quark-antiquark interaction potential". In: *Physica Scripta* 85 (2012), pp. 1–4.

[24] E. Ibekwe et al. “Bound State Solution of Radial Schrodinger Equation for the Quark-Antiquark Interaction Potential”. In: *Iranian Journal of Science and Technology* (2020).

[25] D. Entem & F. Fernandez J. Segovia P. Ortega. “Bottomonium spectrum revisited”. In: *Physical Review D* 93 (2016), pp. 1–27.

[26] E. Bloom & G. Feldman. “Quarkonium”. In: *Scientific American* 246 (1982), pp. 66–77.

[27] W. Deng et al. “Spectrum and electromagnetic transitions of bottomonium”. In: *Physical Review D* 95 (2017), pp. 1–17.

[28] S. Godfrey & K. Moats. “Bottomonium mesons and strategies for their observation”. In: *Physical Review D* 92 (2015), pp. 1–39.

[29] M. Tanabashi et al. (Particle Data Group). “*Upsilon* (1S)”. In: *Physics Review D* 98 (2018), pp. 1–21.

[30] L. Gallegos. “PhD thesis in progress at the University of Sonora”. Unpublished Manuscript. 2021.

[31] N. Filipovic. “Bottomonium measurements in pp, pPb and PbPb using the CMS detector”. In: *Journal of Physics: Conference Series* 612 (2015), pp. 1–4.

[32] Bob McElrath. “Quarkonium decays as a sensitive probe of dark matter”. In: *Physics Letters D* 72 (2005), pp. 1–9.

[33] S. Theisen & J. Silk M. Srednicki. “Cosmic quarkonium: A probe of dark matter”. In: *Physical Review Letters* 56 (1985), pp. 263–265.

[34] T. Matsui & H. Satz. “J/Ψ suppresion by quark-gluon plasma formation”. In: *Physics Letters B* 178 (1986), pp. 416–422.

[35] S. Sarkar & H. Satz & B. Sinha. *The Physics of the Quark-Gluon Plasma*. Berlin, Germany: Springer-Verlag, 2010. ISBN: 9783642022852.

[36] R. Cahn & G. Goldhaber. *The experimental foundations of particle physics*. 2nd ed. New York, New York, USA: Cambridge University Press, 2009. ISBN: 9780521521475.

[37] M. Jacob. “Une brève histoire du CERN”. In: *Bulletin de la société francaise de physique* 147 (2005), pp. 17–20.

[38] C. Smith. “Genesis of the Large Hadron Collider”. In: *Philosophical Transactions A* 373 (2015), pp. 1–11.

[39] L. Evans & P. Bryant. “LHC Machine”. In: *Journal of Instrumentation* (2008), pp. 1–165.

[40] S. Myers. “The Large Hadron Collider 2008-2013”. In: *International Journal of Modern Physics* 28 (2013), pp. 1–65.

[41] CERN. *The CERN accelerator complex - 2019*. Available at `https://cds.cern.ch/record/2684277` (30/08/2021).

[42] CMS Collaboration. “The CMS experiment at the CERN LHC”. In: *Journal of Instrumentation* (2008), pp. 1–362.

[43] CMS Collaboration. *The Compact Muon Solenoid Technical Proposal*. Geneva, Switzerland: CERN, 1994. ISBN: 9290830689.

[44] G. Perez. “Unitarization Models for Vector Boson Scattering at the LHC”. PhD thesis. Karlsruhe, Germany, 2018.

[45] A. Baden. “Jets and Kinematics in Hadronic Collisions”. In: *International Journal of Moden Physics* 13 (1998), pp. 1817–1845.

[46] CMS Collaboration. “A new Boson with a Mass of $125GeV$ Observed with the CMS Experiment at the Large Hadron Collider”. In: *Science* 338 (2012), pp. 1569–1575.

[47] CMS Collaboration. “Particle-flow reconstruction and global event description with the CMS detector”. In: *Journal of Instrumentation* (2017), pp. 1–87.

[48] T. Muller & CMS Collaboration. “The Compact Muon Solenoid and its Physics”. In: *American Institute of Physics Conference Proceedings* 357 (1996), pp. 469–488.

[49] F. Thyssen. “Performance of the Resistive Plate Chambers in the CMS experiment”. In: *Journal of Instrumentation* (2012), pp. 1–9.

[50] D. Orbaker & CMS Collaboration. “Fast simulation of the CMS Detector”. In: *Journal of Physics: Conference Series* 219 (2010), pp. 1–8.

[51] S. Banerjee & I. González & V. Lefébure. “CMS simulation software using Geant4”. In: *CMS Note* 72 (1999), pp. 1–9.

[52] S. Banerjee & CMS Collaboration. “CMS Simulation Software”. In: *Journal of Physics: Conference Series* 396 (2012), pp. 1–9.

[53] Pythia Collaboration. *About PYTHIA*. Available at `https://pythia.org/about/` (18/02/2022).

[54] G. Whitesides. *8.882 LHC Physics. Experimental Methods and Measurements: Efficiency and Acceptance*. Available at `http://web.mit.edu/8.882/www/material/lecture_15.pdf` (06/09/2021).

[55] B. Schutz. *A First Course in General Relativity*. 2nd ed. New York, New York, USA: Cambridge University Press, 2009. ISBN: 9780521887052.

[56] P. Tipler & R. LLewelyn. *Modern Physics*. 5th ed. New York, New York, USA: CW. H. Freeman and Company, 2008. ISBN: 9780716775508.

[57] CERN ROOT. *About ROOT*. Available at `https://root.cern/about/` (06/09/2021).

[58] Y. Kim et al. “Nuclear Modification Factor of Υ(nS) in PbPb Collisions at $\sqrt{s} = 5.02TeV$”. In: *The Compact Muon Solenoid Experiment Analysis Note* 354 (2016), pp. 1–81.

[59] C. Flores. “Strong Suppresion of Υ Excited States in $Pb+Pb$ Collisions at $\sqrt{s_{NN}} = 5.02TeV$ with the CMS Detector”. PhD thesis. Davis, California, USA, 2017.

[60] CMS Collaboration. “Measurement of nuclear modification factors of $\Upsilon(1S)$, $\Upsilon(2S)$, and $\Upsilon(3S)$ mesons in $PbPb$ collisions at $\sqrt{s_{NN}} = 5.02TeV$”. In: *Physics Letters B* 790 (2013), pp. 270–293.

[61] GeoGebra Institute. *Calculator*. Available at `https://www.geogebra.org/calculator` (20/09/2021).

[62] CERN. “Measurement of ϕ meson prodition in p + p interactions at 40, 80 and 158 GeV/c with the NA61/SHINE spectrometer at the CERN SPS”. In: *European Physics Journal C* 165 (2019), pp. 1–26.

[63] G. Falmagne. “Tag-and-probe low-p_T 5 TeV 2017: How-To for analyzers”. Unpublished Manuscript from CMS collaboration. 2019.